

Multi-View Clustering Meets High-Dimensional Mixed Data: A Fusion Regularized Method

Xiangru Xing, Yan Li, Xin Wang, Huangyue Chen, and Xianchao Xiu, *Member, IEEE*

Abstract—Multi-view clustering leverages consistent and complementary information across multiple views to provide more comprehensive insights than analysis of single-view data. However, the heterogeneity and redundancy of high-dimensional mixed multi-view data pose significant challenges to the existing clustering techniques. In this paper, we propose a novel multi-view fusion regularized clustering method with adaptive group sparsity, enabling reliable clustering while effectively capturing local features. Technically, for multi-view data with mixed features exhibiting different distributions, different losses or divergence metrics are considered with a collective fusion penalty to obtain common groups. Moreover, the non-convex group sparsity consisting of inter-group sparsity and intra-group sparsity is utilized to screen informative features, thereby enhancing the robustness. Furthermore, we develop an effective proximal alternating direction method of multipliers (ADMM) and each subproblem admits a closed-form solution. It is rigorously proven that this algorithm globally converges to a Karush-Kuhn-Tucker (KKT) point, while establishing the equivalence between local minimum points and KKT points within a certain region. Extensive numerical experiments on both simulated and real data validate the superior performance of the presented method in clustering accuracy and feature selection.

Index Terms—Multi-view clustering, mixed data, group sparsity, feature selection, alternating direction method of multipliers.

I. INTRODUCTION

IN the field of images and videos, multi-view data are ubiquitous [1]. For instance, images can be characterized from multiple views such as the texture features extracted by local binary pattern (LBP), the shape features obtained through the histogram of oriented gradient (HOG), and the color features calculated via color moment (CMT). Although multi-view data are heterogeneous, there are certain potential connections between them [2]. A large number of studies have demonstrated that multi-view learning can fully exploit the diversity and complementarity of these views for better efficiency and robustness [3]. Currently, it has become a very

promising field, with wide applications in finger biometrics [4], multimedia understanding [5], image segmentation [6], and image recognition [7].

However, multi-view data collected from different sources usually have two prominent characteristics: *mixed types* and *high dimensionality*. For the former, its samples contain multiple feature sets of varying types, such as continuous, count, binary, and categorical. This kind of mixed-type data is often termed mixed multi-view data [8], which is prevalent in wide fields like remote sensing, integrated genomics, multimodal imaging, and online advertising. Although numerous techniques (e.g., [9], [10]) have been developed in the past decades, there remain few methods capable of directly performing joint analysis on mixed multi-view data [11]. For the latter, one classical technique for reducing the dimensionality is to perform principal component analysis (PCA) [12], *t*-distributed stochastic neighbor embedding (*t*-SNE) [13], non-negative matrix factorization (NMF) [14] or projection [15] before clustering. However, such methods may lead to results that do not directly illustrate the importance of features. Moreover, in practical scenarios, determining the rank of factors is acknowledged to be extremely challenging and usually has a profound impact on the final results [16].

In this paper, we attempt to exploit mixed multi-view data to cluster common samples more effectively and select informative features to distinguish the inherent group structures. Specifically, we present a innovative group-sparsity-based multi-view fusion regularized clustering that can integrate mixed-type data with distinct data-specific losses, cluster co-samples using a collective fusion penalty, as well as select locally relevant features. Notably, in contrast to other prevalent multi-view clustering techniques, such as multi-view *K*-means clustering [17], multi-view subspace clustering [18], and multi-view spectral clustering [19], our proposed method does not require prior knowledge regarding the number of clusters. To address non-Gaussian scenarios more effectively, a comprehensive loss function is formulated based on the characteristics of each view. Furthermore, inter-group sparsity with $l_{2,0}$ -norm [20], [21], a component of group sparsity, is devised to provide a more intuitive explanation than its approximate method called Lasso in [22], [23]. As another integral part of the group sparsity, the intra-group sparsity with l_0 -norm [24], [25], is ubiquitous in real-world applications. Therefore, we develop a group sparsity term, i.e., $l_{2,0}$ -norm plus l_0 -norm, that aims to select relevant features with useful data points. Meanwhile, the non-convexity and non-smoothness of group sparsity bring great challenges to model analysis. Even so, we design an effective optimization algorithm and provide a solid

This work was supported by the National Natural Science Foundation of China under Grant 12071022 and 12371306, and the Innovative Talent Project of Karamay under Grant XQZX20240078. (*Corresponding author: Xin Wang.*)

Xiangru Xing and Xin Wang are with the School of Mathematics and Statistics, Beijing Jiaotong University, Beijing 100044, China (e-mail: 21118025@bjtu.edu.cn; xinwang2@bjtu.edu.cn).

Yan Li is with the School of Insurance and Economics, University of International Business and Economics, Beijing 100029, China (e-mail: liyan2010@uibe.edu.cn).

Huangyue Chen is with the School of Mathematics and Information Science, Guangxi University, Nanning 530004, China (e-mail: hychen2024@gxu.edu.cn).

Xianchao Xiu is with the School of Mechatronic Engineering and Automation, Shanghai University, Shanghai 200444, China (e-mail: xcxiu@shu.edu.cn).

convergence theory guarantee.

Compared with the existing works, our main contributions are outlined below.

- 1) For high-dimensional mixed data, we present a general multi-view clustering model with inter-group sparsity and intra-group sparsity, which has not been considered before. This model can simultaneously and efficiently implement clustering and feature selection, and is therefore more robust than traditional clustering models.
- 2) For the proposed non-convex and non-smooth model, we develop a proximal alternating direction method of multipliers (ADMM)-based algorithm. Fortunately, all the resulting subproblems have closed-form solutions, thus achieving an efficient optimization algorithm.
- 3) By using the spatial decomposition technique, we obtain the equivalence between local minimum points and Karush-Kuhn-Tucker (KKT) points within a specific region, which provides theoretical support for the analysis of convergence. Under mild conditions, we establish the global¹ convergence without applying the existing approximation or smoothing methods [26], [27].
- 4) Numerical experiments on both synthetic data and real data demonstrate that the proposed method outperforms the state-of-the-art fusion regularized clustering model and other advanced clustering methods.

The overview of the remaining article is shown below. Section II briefly reviews the related work. Section III provides our multi-view clustering model and optimization algorithm. The detailed theoretical guarantees are given in Section IV. The experimental results are presented in Section V. Finally, Section VI draws the conclusion.

II. PRELIMINARIES

A. Notations

For a given matrix $\mathbf{A} \in \mathbb{R}^{n \times p}$, $\mathbf{A}_{i\cdot}$, $\mathbf{A}_{\cdot j}$, and \mathbf{A}_{ij} denote its i -th row, j -th column, and (i, j) -th element, respectively. $\|\mathbf{A}\|_F = (\sum_{i=1}^n \sum_{j=1}^p \mathbf{A}_{ij}^2)^{1/2}$ denotes the Frobenius norm. $\|\mathbf{A}\|_{2,0} = \sum_{j=1}^p \mathbb{I}(\|\mathbf{A}_{\cdot j}\|_2 \neq 0)$, $\|\mathbf{A}\|_0 = \sum_{i=1}^n \sum_{j=1}^p \mathbb{I}(\mathbf{A}_{ij} \neq 0)$, where $\mathbb{I}(\cdot)$ is the indicator function. $\|\mathbf{A}_{i\cdot}\|_q = (\sum_{j=1}^p \mathbf{A}_{ij}^q)^{1/q}$ denotes the l_q -norm of vector $\mathbf{A}_{i\cdot}$ with $q \geq 1$. The image space of \mathbf{A} is defined as $\text{Im}(\mathbf{A}) = \{\mathbf{A}\mathbf{x} \mid \mathbf{x} \in \mathbb{R}^p\}$. Besides, $\lambda_+(\mathbf{A}^\top \mathbf{A})$ and $\lambda_{\max}(\mathbf{A}^\top \mathbf{A})$ denote the smallest positive eigenvalue and the largest eigenvalue of $\mathbf{A}^\top \mathbf{A}$. For \mathbf{A} and \mathbf{B} of any dimension, $\text{Diag}(\mathbf{A}, \mathbf{B})$ is a block diagonal matrix consisting of them. \mathbf{e}_n is an n -dimensional column vector with components equal to 1. If not specified, \mathbf{I} and $\mathbf{0}$ are successively the identity matrix and the zero matrix, both of which are of the appropriate dimension.

Let $f: \mathcal{A} \rightarrow (-\infty, +\infty]$ be a proper closed function. For $\mathbf{A} \in \mathcal{A}$, the proximal mapping $\text{Prox}_{\tau f}(\cdot)$ is defined by

$$\text{Prox}_{\tau f}(\mathbf{A}) = \arg \min_{\mathbf{U} \in \mathcal{A}} \left\{ \tau f(\mathbf{U}) + \frac{1}{2} \|\mathbf{U} - \mathbf{A}\|_F^2 \right\}. \quad (1)$$

We list the proximal mappings involved in this paper in Table I. More functions and associated proximal mappings can be found in [28].

TABLE I
PROXIMAL MAPPINGS FOR SELECTED FUNCTIONS.

$f(\cdot)$	$\text{Prox}_{\tau f}(\mathbf{A})$
$\ \cdot\ _{2,1}$	$[\text{Prox}_{\tau \ \cdot\ _{2,1}}(\mathbf{A})]_{i\cdot} = \left(1 - \frac{\tau}{\max\{\ \mathbf{A}_{i\cdot}\ _2, \tau\}}\right) \mathbf{A}_{i\cdot}$
$\ \cdot\ _{2,0}$	$[\text{Prox}_{\tau \ \cdot\ _{2,0}}(\mathbf{A})]_{i\cdot} = \begin{cases} \mathbf{A}_{i\cdot}, & \ \mathbf{A}_{i\cdot}\ _2 > \sqrt{2\tau} \\ \mathbf{A}_{i\cdot} \text{ or } 0, & \ \mathbf{A}_{i\cdot}\ _2 = \sqrt{2\tau} \\ 0, & \ \mathbf{A}_{i\cdot}\ _2 < \sqrt{2\tau} \end{cases}$
$\ \cdot\ _0$	$[\text{Prox}_{\tau \ \cdot\ _0}(\mathbf{A})]_{ij} = \begin{cases} \mathbf{A}_{ij}, & \mathbf{A}_{ij} > \sqrt{2\tau} \\ \mathbf{A}_{ij} \text{ or } 0, & \mathbf{A}_{ij} = \sqrt{2\tau} \\ 0, & \mathbf{A}_{ij} < \sqrt{2\tau} \end{cases}$

B. Related Work

The fusion regularized clustering (also known as sum-of-norms clustering, convex clustering, and clusterpath) was initially proposed by [29], whose fundamental model is

$$\min_{\mathbf{U}} \frac{1}{2} \sum_{i=1}^n \|\mathbf{X}_{i\cdot} - \mathbf{U}_{i\cdot}\|_2^2 + \eta \sum_{l_1 < l_2} \omega_{l_1 l_2} \|\mathbf{U}_{l_1\cdot} - \mathbf{U}_{l_2\cdot}\|_q, \quad (2)$$

where $\mathbf{X} \in \mathbb{R}^{n \times p}$ denotes a known matrix with n observations and p features, $\mathbf{U} \in \mathbb{R}^{n \times p}$ is a centroid matrix, η is a positive tuning parameter, which is introduced to balance the model fit and the number of clusters. As a result, by adjusting η , the number of clusters can be automatically determined to best describe the data without the need for prior specification [30]. In addition, $\|\cdot\|_q$ is the l_q -norm with $q \in \{1, 2, \infty\}$ commonly considered. For example, l_1 -norm loss is utilized in the presence of outliers. Given a positive constant ϕ , the fusion weight $\omega_{l_1 l_2}$ is defined as

$$\omega_{l_1 l_2} = \begin{cases} \exp(-\phi d(\mathbf{X}_{i\cdot}, \mathbf{X}_{j\cdot})), & \text{if } (l_1, l_2) \in \epsilon, \\ 0, & \text{otherwise,} \end{cases} \quad (3)$$

where $d(\mathbf{X}_{i\cdot}, \mathbf{X}_{j\cdot}) = \|\mathbf{X}_{l_1\cdot} - \mathbf{X}_{l_2\cdot}\|_2^2$ and $\epsilon = \cup_{l_1=1}^n \{(l_1, l_2) \mid \mathbf{X}_{l_2\cdot} \text{ is among } \mathbf{X}_{l_1\cdot}\text{'s } K\text{-nearest neighbors, } 1 \leq l_1 < l_2 \leq n\}$.

Although fusion regularized clustering has desirable theoretical results and good computational performance [31], the clustering performance may be damaged in high-dimensional cases with more features than observations. To address this, [32] proposed sparse convex clustering with the inter-group Lasso penalty, i.e.,

$$\min_{\mathbf{U}} \frac{1}{2} \sum_{i=1}^n \|\mathbf{X}_{i\cdot} - \mathbf{U}_{i\cdot}\|_2^2 + \eta \sum_{l_1 < l_2} \omega_{l_1 l_2} \|\mathbf{U}_{l_1\cdot} - \mathbf{U}_{l_2\cdot}\|_q + \beta \sum_{j=1}^p \bar{\beta}_j \|\mathbf{U}_{\cdot j}\|_2, \quad (4)$$

where $\beta > 0$ controls the number of informative features, and $\bar{\beta}_j$ determines the importance ratio of each feature. In this way, the cluster centers are shrunk towards zero and relevant features are selected. On this basis, [33] considered the intra-group sparse penalty with l_1 -norm to enhance the ability of feature selection. However, these fusion regularized clustering models endowed with feature selection capabilities are only valid when the mean of the data is precisely zero. Otherwise, the lasso penalty terms will select wrong features, thereby causing the model to generate incorrect cluster centers.

¹“Global” here means regardless of where the initial point is.

For mixed multi-view data, the above fusion regularized clustering models in (2) and (4) exhibit relatively poor performance [34]. Subsequently, considering the characteristics of mixed data, several scholars adopted alternative losses, such as Bernoulli log-likelihood [9], Huber loss [35], and others [10], [36], with the aim of improving the accuracy of data fitting. Recently, [23] proposed an adaptive inter-group Lasso penalty to select features by shrinking them towards their loss-specific centers, which is given by

$$\min_{\mathbf{U}^1, \mathbf{U}^2, \dots, \mathbf{U}^K} \sum_{k=1}^K \zeta_k \ell_k(\mathbf{X}^k, \mathbf{U}^k) + \eta \sum_{\iota_1 < \iota_2} \omega_{\iota_1 \iota_2} \times \sqrt{\sum_{k=1}^K \|\mathbf{U}_{\iota_1}^k - \mathbf{U}_{\iota_2}^k\|_2^2} + \beta \sum_{k=1}^K \sum_{j=1}^{p_k} \bar{\beta}_j^k \|\mathbf{U}_{\cdot j}^k - \bar{\mathbf{x}}_j^k \cdot \mathbf{e}_n\|_2, \quad (5)$$

where K represents the number of data sources. For the k -th view, $\mathbf{X}^k \in \mathbb{R}^{n \times p_k}$ is the k -th data matrix with n observations and p_k features, $\mathbf{U}^k \in \mathbb{R}^{n \times p_k}$ is the corresponding centroid, ζ_k is determined in advance by the user with $\sum_{k=1}^K \zeta_k = 1$, the k -th loss function $\ell_k(\mathbf{X}^k, \mathbf{U}^k)$ is appropriately chosen depending on the type of \mathbf{X}^k . In addition, $\bar{\mathbf{x}}^k = \arg \min_{\mathbf{U}^k} \ell_k(\mathbf{X}^k, \mathbf{U}^k)$ is a loss-specific center. For instance, $\ell_k(\mathbf{X}^k, \mathbf{U}^k) = \sum_{i=1}^n \|\mathbf{X}_i^k - \mathbf{U}_i^k\|_2^2$ for Gaussian data, then $\bar{\mathbf{x}}^k = \sum_{i=1}^n \mathbf{X}_i^k / n$. See [23, Table 1] for additional examples. It is worth noting that (5) considers the fusion regularized clustering of mixed multi-view data for the first time, capturing the inherent structure of multiple data types while being more universal.

III. THE PROPOSED METHOD

In this section, we start with the presentation of our new model, followed by its optimization algorithm.

A. New Model

To deal with multi-view data with *mixed types* and *high dimensionality*, we construct a multi-view fusion regularized clustering model with group sparsity defined as

$$\min_{\mathbf{U}} \sum_{k=1}^K \zeta_k \ell_k(\mathbf{X}^k, \mathbf{U}^k) + \eta \sum_{\iota \in \epsilon} w_{\iota} \|(\mathbf{DU})_{\cdot \iota}\|_2 + \beta \left[(1 - \theta) \sum_{k=1}^K \|(\mathbf{U}^k - \bar{\mathbf{X}}^k) \bar{\beta}^k\|_{2,0} + \theta \|\mathbf{U} - \bar{\mathbf{X}}\|_0 \right]. \quad (6)$$

where $\mathbf{U} = [\mathbf{U}^1, \mathbf{U}^2, \dots, \mathbf{U}^K] \in \mathbb{R}^{n \times p}$ is the whole centroid matrix with $\mathbf{U}^k \in \mathbb{R}^{n \times p_k}$. Next, we will explain each item in detail.

- The first term plays the role of data fitting. Loss function $\ell_k(\mathbf{X}^k, \mathbf{U}^k)$ is convex and possibly non-smooth for the k -th data view whose type is chosen appropriately according to the characteristics of data \mathbf{X}^k . Here, we suppose that the non-smooth loss $\ell_k(\mathbf{X}^k, \mathbf{U}^k) = \ell_k(\mathbf{X}^k - \mathbf{U}^k)$, where ℓ_k is distance-based such as Manhattan distance, Chebychev distance, and square-root-loss. Actually, it follows a similar idea as (5).
- The second term facilitates the rows' differences of concatenated centroid $[\mathbf{U}^1, \mathbf{U}^2, \dots, \mathbf{U}^K]$ to shrink

towards zero, thereby inducing a clustering behavior. In detail, $(\mathbf{DU})_{\cdot \iota} = \mathbf{U}_{\iota_1} - \mathbf{U}_{\iota_2}$ for edge $\iota = (\iota_1, \iota_2)$ and the directed difference matrix $\mathbf{D} \in \mathbb{R}^{|\epsilon| \times n}$. We use l_2 -norm to promote the fusion of the whole rows of similar observations simultaneously and to ensure rotation invariance. Under the action of the sparse fusion weight ω_{ι} , this term enforces the group structure of the ι_1 -th row of \mathbf{U}^k to be the identical for all $k \in [K]$. We consider that $\mathbf{X}_{\iota_1 \cdot}$ and $\mathbf{X}_{\iota_2 \cdot}$ belong to the same cluster if $\mathbf{U}_{\iota_1 \cdot} = \mathbf{U}_{\iota_2 \cdot}$. Unlike convex clustering in (2) and (4), the Gower distance

$$d(\mathbf{X}_{\iota_1 \cdot}, \mathbf{X}_{\iota_2 \cdot}) = \sum_{k=1}^K \sum_{j=1}^{p_k} \frac{d_{\iota_1 \iota_2 j}^k}{\sum_{k=1}^K p_k} \quad (7)$$

is introduced for clustering mixed multi-view data [37], [38], where

$$d_{\iota_1 \iota_2 j}^k = \frac{|\mathbf{X}_{\iota_1 j}^k - \mathbf{X}_{\iota_2 j}^k|}{\max_{\iota_1, \iota_2} |\mathbf{X}_{\iota_1 j}^k - \mathbf{X}_{\iota_2 j}^k|}. \quad (8)$$

- The last two terms are enforced to achieve feature selection. Here, $\bar{\mathbf{X}}^k = [\bar{\mathbf{x}}_{\cdot 1}^k \cdot \mathbf{e}_n, \bar{\mathbf{x}}_{\cdot 2}^k \cdot \mathbf{e}_n, \dots, \bar{\mathbf{x}}_{\cdot p_k}^k \cdot \mathbf{e}_n]$ in which $\bar{\mathbf{x}}^k$ is a loss-specific center. $\theta \in [0, 1]$ is a parameter to balance the inter-group sparsity and intra-group sparsity. $\bar{\beta}^k = \text{Diag}(\bar{\beta}_1^k, \bar{\beta}_2^k, \bar{\beta}_3^k, \dots, \bar{\beta}_{p_k}^k)$ is the feature weight with $\bar{\beta}_j^k > 0, j \in [p_k]$. The impact of parameters η, β , and θ will be explained in Section V.

We would also like to point out that although the Lasso method can reveal the sparse structure of solutions, it may lead to biased estimates as illustrated in [39]. Different from the multi-view fusion regularized clustering with Lasso penalty discussed in [23], [33], our proposed model considers the group sparsity that is the combination of $l_{2,0}$ -norm and l_0 -norm. In feature selection, the group sparsity provides a more intuitive explanation because l_0 -norm is the primordial method for characterizing sparsity. In addition, group sparsity has great flexibility by adjusting the parameters β and θ .

B. Optimization Algorithm

Due to its non-differentiability with respect to the variable \mathbf{U} , (6) poses great difficulties to solution and convergence analysis. Therefore, it is necessary to develop an effective algorithm with rigorous convergence proof.

Define $\tau := \{k \in [K] \mid \ell_k \text{ is differentiable}\}$, where $\bar{\tau}$ is the complement of τ to the set $[K]$, $\kappa := \sum_{k \in \tau} p_k$, $\bar{\kappa} := \sum_{k \in \bar{\tau}} p_k$. We further introduce four slack variables $\mathbf{V}^{\bar{\tau}} \in \mathbb{R}^{n \times \bar{\kappa}}$, $\mathbf{E} \in \mathbb{R}^{n \times p}$, $\mathbf{F} \in \mathbb{R}^{n \times p}$, and $\bar{\mathbf{F}} \in \mathbb{R}^{n \times p}$ for ease of solving. A proximal term in the $\mathbf{U}^{\bar{\tau}}$ -subproblem is added to improve the convergence behavior. Let $L_{\tau}(\mathbf{U}^{\tau}) = \sum_{k \in \tau} \zeta_k \ell_k(\mathbf{X}^k, \mathbf{U}^k)$, $q(\mathbf{V}^{\bar{\tau}}) = \sum_{k \in \bar{\tau}} \zeta_k \ell_k(\mathbf{V}^k)$, $p(\mathbf{E}) = \eta \sum_{\iota \in \epsilon} w_{\iota} \|(\mathbf{E})_{\cdot \iota}\|_2$, $r_1(\mathbf{F}) = \sum_{k=1}^K \beta(1 - \theta) \|\mathbf{F}^k \bar{\beta}^k\|_{2,0}$, $r_2(\bar{\mathbf{F}}) = \sum_{k=1}^K \beta \theta \|\bar{\mathbf{F}}^k\|_0$. Then, problem (6) can be equivalently transformed to

$$\begin{aligned} \min_{\mathbf{U}, \mathbf{V}^{\bar{\tau}}, \mathbf{E}, \mathbf{F}, \bar{\mathbf{F}}} & L_{\tau}(\mathbf{U}^{\tau}) + q(\mathbf{V}^{\bar{\tau}}) + p(\mathbf{E}) + r_1(\mathbf{F}) + r_2(\bar{\mathbf{F}}) \\ \text{s.t.} & \mathbf{DU} = \mathbf{E}, \quad \mathbf{X}^{\bar{\tau}} - \mathbf{U}^{\bar{\tau}} = \mathbf{V}^{\bar{\tau}}, \\ & \mathbf{U} - \bar{\mathbf{X}} = \mathbf{F}, \quad \mathbf{U} - \bar{\mathbf{X}} = \bar{\mathbf{F}}, \end{aligned} \quad (9)$$

where $\mathbf{U}^\tau \in \mathbb{R}^{n \times \kappa}$ and $\mathbf{U}^{\bar{\tau}} \in \mathbb{R}^{n \times \bar{\kappa}}$ are the centroid matrices corresponding to \mathbf{X}^τ and $\mathbf{X}^{\bar{\tau}}$, and $\mathbf{V}^{\bar{\tau}}$ is the horizontal concatenation matrix of $\{\mathbf{V}^k\}_{k \in \bar{\tau}}$.

Given $\sigma > 0$, the augmented Lagrangian function of (9) is

$$\begin{aligned} \mathcal{L}_\sigma(\mathbf{U}, \mathbf{V}^{\bar{\tau}}, \mathbf{E}, \mathbf{F}, \bar{\mathbf{F}}; \mathbf{Q}^{\bar{\tau}}, \mathbf{H}, \mathbf{G}, \bar{\mathbf{G}}) \\ = L_\tau(\mathbf{U}^\tau) + q(\mathbf{V}^{\bar{\tau}}) + p(\mathbf{E}) + r_1(\mathbf{F}) + r_2(\bar{\mathbf{F}}) \\ + \Psi_1(\mathbf{V}^{\bar{\tau}}) + \Psi_2(\mathbf{E}) + \Psi_3(\mathbf{F}) + \Psi_4(\bar{\mathbf{F}}), \end{aligned} \quad (10)$$

where $\mathbf{H} \in \mathbb{R}^{n \times p}$, $\mathbf{G} \in \mathbb{R}^{n \times p}$, $\mathbf{Q}^{\bar{\tau}} \in \mathbb{R}^{n \times \bar{\kappa}}$ and $\bar{\mathbf{G}} \in \mathbb{R}^{n \times p}$ are the Lagrange multipliers, and

$$\begin{aligned} \Psi_1(\mathbf{V}^{\bar{\tau}}) &= \langle \mathbf{Q}^{\bar{\tau}}, \mathbf{U}^{\bar{\tau}} + \mathbf{V}^{\bar{\tau}} - \mathbf{X}^{\bar{\tau}} \rangle + \frac{\sigma}{2} \|\mathbf{U}^{\bar{\tau}} + \mathbf{V}^{\bar{\tau}} - \mathbf{X}^{\bar{\tau}}\|_{\bar{F}}^2, \\ \Psi_2(\mathbf{E}) &= \langle \mathbf{H}, \mathbf{D}\mathbf{U} - \mathbf{E} \rangle + \frac{\sigma}{2} \|\mathbf{D}\mathbf{U} - \mathbf{E}\|_{\bar{F}}^2, \\ \Psi_3(\mathbf{F}) &= \langle \mathbf{G}, \mathbf{U} - \bar{\mathbf{X}} - \mathbf{F} \rangle + \frac{\sigma}{2} \|\mathbf{U} - \bar{\mathbf{X}} - \mathbf{F}\|_{\bar{F}}^2, \\ \Psi_4(\bar{\mathbf{F}}) &= \langle \bar{\mathbf{G}}, \mathbf{U} - \bar{\mathbf{X}} - \bar{\mathbf{F}} \rangle + \frac{\sigma}{2} \|\mathbf{U} - \bar{\mathbf{X}} - \bar{\mathbf{F}}\|_{\bar{F}}^2. \end{aligned} \quad (11)$$

As illustrated in [40], the convergence of ADMM with multiple blocks cannot be guaranteed. Fortunately, (9) can be rewritten into a 2-block ADMM by defining

$$\begin{aligned} \mathbf{\Upsilon}_1 &= (\mathbf{V}^{\bar{\tau}}, \mathbf{F}, \bar{\mathbf{F}}, \mathbf{E}), \\ \mathbf{\Upsilon}_2 &= (\mathbf{Q}^{\bar{\tau}}, \mathbf{G}, \bar{\mathbf{G}}, \mathbf{H}). \end{aligned} \quad (12)$$

To this end, we can alternately minimize the primal variables among $\mathbf{\Upsilon}_1$ and \mathbf{U} , and then update the multipliers $\mathbf{\Upsilon}_2$. Given the current iteration point $\mathbf{\Upsilon}^{(t)}$, then the next iteration point $(\mathbf{\Upsilon}_1^{(t+1)}, \mathbf{U}^{(t+1)}, \mathbf{\Upsilon}_2^{(t+1)})$ is generated below.

1) Update $\mathbf{V}^{\bar{\tau}}$ via:

$$\min_{\mathbf{V}^{\bar{\tau}}} q(\mathbf{V}^{\bar{\tau}}) + \Psi_1(\mathbf{V}^{\bar{\tau}}). \quad (13)$$

Due to the divisibility of function $q(\cdot)$, we can obtain its closed-form solution for $\forall k \in \bar{\tau}$, that is

$$\mathbf{V}^{k(t+1)} \in \text{Prox}_{\zeta_k \ell_k / \sigma}(\mathbf{X}^k - \mathbf{U}^{k(t)} + \frac{1}{\sigma} \mathbf{Q}^{k(t)}), \quad (14)$$

where Prox is defined

2) Update \mathbf{F} via:

$$\min_{\mathbf{F}} r_1(\mathbf{F}) + \Psi_3(\mathbf{F}). \quad (15)$$

Given the divisibility of function $r_1(\cdot)$, its closed-form solution can be described by

$$\mathbf{F}^{k(t+1)} \in \text{Prox}_{r_3 / \sigma}(\mathbf{U}^{k(t)} - \bar{\mathbf{X}}^k + \frac{1}{\sigma} \mathbf{G}^{k(t)}), \quad (16)$$

where $r_3(\mathbf{F}^k) = \beta(1 - \theta) \|\mathbf{F}^k \bar{\beta}^k\|_{2,0}$ for $\forall k \in [K]$.

3) Update $\bar{\mathbf{F}}$ via:

$$\min_{\bar{\mathbf{F}}} r_2(\bar{\mathbf{F}}) + \Psi_4(\bar{\mathbf{F}}). \quad (17)$$

Similarly, in view of the divisibility of function $r_2(\cdot)$, its closed-form solution is

$$\bar{\mathbf{F}}^{k(t+1)} \in \text{Prox}_{r_4 / \sigma}(\mathbf{U}^{k(t)} - \bar{\mathbf{X}}^k + \frac{1}{\sigma} \bar{\mathbf{G}}^{k(t)}), \quad (18)$$

where $r_4(\bar{\mathbf{F}}^k) = \beta\theta \|\bar{\mathbf{F}}^k\|_0$ for $\forall k \in [K]$.

Algorithm 1 Proximal ADMM for solving (9)

Initialization: Choose $(\mathbf{\Upsilon}_1^{(0)}, \mathbf{U}^{(0)}, \mathbf{\Upsilon}_2^{(0)})$ and $\sigma > 0$
while not converged **do**

for $t = 0, 1, 2, \dots$, **do**

Step 1. Compute $\mathbf{\Upsilon}_1^{(t+1)}$:

 Update $\mathbf{V}^{k(t+1)}$ by (14)

 Update $\mathbf{F}^{k(t+1)}$ by (16)

 Update $\bar{\mathbf{F}}^{k(t+1)}$ by (18)

 Update $\mathbf{E}^{k(t+1)}$ by (20)

Step 2. Compute $\mathbf{U}^{(t+1)}$

if $k \in \tau$, **then** update $\mathbf{U}^{k(t+1)}$ by (22)

else if $k \in \bar{\tau}$, **then** update $\mathbf{U}^{k(t+1)}$ by (25)

end if

Step 3. Compute $\mathbf{\Upsilon}_2^{(t+1)}$

 Update $\mathbf{Q}^{k(t+1)}$ by (26)

 Update $\mathbf{G}^{k(t+1)}$ by (27)

 Update $\bar{\mathbf{G}}^{k(t+1)}$ by (28)

 Update $\mathbf{H}^{k(t+1)}$ by (29)

end for

end while

Output $(\mathbf{\Upsilon}_1^{(t+1)}, \mathbf{U}^{(t+1)}, \mathbf{\Upsilon}_2^{(t+1)})$

4) Update \mathbf{E} via:

$$\min_{\mathbf{E}} p(\mathbf{E}) + \Psi_2(\mathbf{E}). \quad (19)$$

After calculation, its closed-form solution is

$$\mathbf{E}^{(t+1)} \in \text{Prox}_{p/\sigma}(\mathbf{D}\mathbf{U}^{(t)} + \frac{1}{\sigma} \mathbf{H}^{(t)}). \quad (20)$$

5) Update \mathbf{U}^k : Since the loss function $L_\tau(\mathbf{U}^\tau) + L_{\bar{\tau}}(\mathbf{U}^{\bar{\tau}})$ is composed of differentiable loss functions $\ell_k(\mathbf{X}^k, \mathbf{U}^k)$, $k \in \tau$ and non-differentiable loss functions $\ell_k(\mathbf{X}^k - \mathbf{U}^k)$, $k \in \bar{\tau}$. For convenience, we will discuss it in two cases.

(Case I) For $k \in \tau$, we have

$$\min_{\mathbf{U}^k} \ell_k(\mathbf{X}^k, \mathbf{U}^k) + \Psi(\mathbf{\Upsilon}_1^{k(t+1)}), \quad (21)$$

where $\Psi(\mathbf{\Upsilon}_1^{k(t+1)}) = \Psi_1(\mathbf{V}^{k(t+1)}) + \Psi_2(\mathbf{E}^{k(t+1)}) + \Psi_3(\mathbf{F}^{k(t+1)}) + \Psi_4(\bar{\mathbf{F}}^{k(t+1)})$. Then, we can directly obtain that closed-form solution by solving

$$\mathbf{U}^{k(t+1)} = \arg \min_{\mathbf{U}^k} \{\ell_k(\mathbf{X}^k, \mathbf{U}^k) + \Psi(\mathbf{\Upsilon}_1^{k(t+1)})\}. \quad (22)$$

(Case II) For $k \in \bar{\tau}$, we have

$$\min_{\mathbf{U}^k} \Psi(\mathbf{\Upsilon}_1^{k(t+1)}). \quad (23)$$

To guarantee and speed up the convergence, we add a proximal term to (23). Then, it can be transformed into

$$\min_{\mathbf{U}^k} \Psi(\mathbf{\Upsilon}_1^{k(t+1)}) + \frac{\gamma}{2} \|\mathbf{U}^k - \mathbf{U}^{k(t)}\|_{\bar{F}}^2. \quad (24)$$

According to the Fermat's theorem, we can acquire the closed-form solution as

$$\begin{aligned} \mathbf{U}^{k(t+1)} &= \left((3 + \frac{\gamma}{\sigma})\mathbf{I} + \mathbf{D}^\top \mathbf{D} \right)^{-1} (\mathbf{X}^k - \mathbf{V}^{k(t+1)} \\ &\quad - \frac{1}{\sigma} \mathbf{Q}^{k(t)} + \mathbf{D}^\top \mathbf{E}^{k(t+1)} - \frac{1}{\sigma} \mathbf{H}^{k(t)} + 2\bar{\mathbf{X}}^k \\ &\quad + \mathbf{F}^{k(t+1)} - \frac{1}{\sigma} \mathbf{G}^{k(t)} + \bar{\mathbf{F}}^{k(t+1)} \\ &\quad - \frac{1}{\sigma} \bar{\mathbf{G}}^{k(t)} + \frac{\gamma}{\sigma} \mathbf{U}^{k(t)}). \end{aligned} \quad (25)$$

6) *Update Multipliers:* For $\forall k \in \bar{\tau}$, we have

$$\mathbf{Q}^{k(t+1)} = \mathbf{Q}^{k(t)} + \sigma(\mathbf{X}^k - \mathbf{U}^{k(t+1)} - \mathbf{V}^{k(t+1)}). \quad (26)$$

For $\forall k \in [K]$, we get

$$\mathbf{G}^{k(t+1)} = \mathbf{G}^{k(t)} + \sigma(\mathbf{U}^{k(t+1)} - \bar{\mathbf{X}}^k - \mathbf{F}^{k(t+1)}), \quad (27)$$

$$\bar{\mathbf{G}}^{k(t+1)} = \bar{\mathbf{G}}^{k(t)} + \sigma(\mathbf{U}^{k(t+1)} - \bar{\mathbf{X}}^k - \bar{\mathbf{F}}^{k(t+1)}), \quad (28)$$

$$\mathbf{H}^{k(t+1)} = \mathbf{H}^{k(t)} + \sigma(\mathbf{D}\mathbf{U}^{k(t+1)} - \mathbf{E}^{k(t+1)}). \quad (29)$$

The horizontally concatenate matrices \mathbf{V}^τ , \mathbf{F} , $\bar{\mathbf{F}}$, \mathbf{U}^τ , and \mathbf{U}^τ are divided into the matrices \mathbf{V}^k , \mathbf{F}^k , $\bar{\mathbf{F}}^k$, and \mathbf{U}^k of each view for separate solution, so as to reduce some computational complexity without affecting the solution accuracy. The specific iterative steps are shown in Algorithm 1.

IV. THEORETICAL GUARANTEE

In this section, we establish the optimization conditions and global convergence analysis.

A. Optimality Conditions

For better describing optimality conditions, we first recast (6) as the following equivalent constrained problem

$$\begin{aligned} \min_{\mathbf{U}, \mathbf{E}, \mathbf{F}} \quad & L_\tau(\mathbf{U}^\tau) + L_{\bar{\tau}}(\mathbf{U}^{\bar{\tau}}) + p(\mathbf{E}) + r(\mathbf{F}) \\ \text{s.t.} \quad & \mathbf{D}\mathbf{U} = \mathbf{E}, \quad \mathbf{U} - \bar{\mathbf{X}} = \mathbf{F}, \end{aligned} \quad (30)$$

where $r(\mathbf{F}) = \sum_{k=1}^K (r_3(\mathbf{F}^k) + r_4(\mathbf{F}^k))$. The Lagrangian function of (30) is given by

$$\begin{aligned} \mathcal{L}(\mathbf{U}, \mathbf{E}, \mathbf{F}; \mathbf{H}, \mathbf{G}) &= L_\tau(\mathbf{U}^\tau) + L_{\bar{\tau}}(\mathbf{U}^{\bar{\tau}}) + p(\mathbf{E}) \\ &\quad + r(\mathbf{F}) + \langle \mathbf{H}, \mathbf{D}\mathbf{U} - \mathbf{E} \rangle + \langle \mathbf{G}, \mathbf{U} - \bar{\mathbf{X}} - \mathbf{F} \rangle. \end{aligned} \quad (31)$$

Definition 1: A point $(\tilde{\mathbf{U}}, \tilde{\mathbf{E}}, \tilde{\mathbf{F}})$ is said to a KKT point of (30) provided that there exist matrices $\tilde{\mathbf{H}} \in \mathbb{R}^{n \times p}$ and $\tilde{\mathbf{G}} \in \mathbb{R}^{n \times p}$ such that

$$\begin{cases} 0 = \nabla L_\tau(\tilde{\mathbf{U}}^\tau) + \mathbf{D}^\top \tilde{\mathbf{H}}^\tau + \tilde{\mathbf{G}}^\tau, \\ 0 \in \partial L_{\bar{\tau}}(\tilde{\mathbf{U}}^{\bar{\tau}}) + \mathbf{D}^\top \tilde{\mathbf{H}}^{\bar{\tau}} + \tilde{\mathbf{G}}^{\bar{\tau}}, \\ 0 \in \partial p(\tilde{\mathbf{E}}) - \tilde{\mathbf{H}}, \\ 0 \in \partial r_3(\tilde{\mathbf{F}}^k) \tilde{\beta}^k + \partial r_4(\tilde{\mathbf{F}}^k) - \tilde{\mathbf{G}}^k, \quad \forall k \in [K], \\ 0 = \mathbf{D}\mathbf{U} - \mathbf{E}, 0 = \mathbf{U} - \bar{\mathbf{X}} - \mathbf{F}. \end{cases} \quad (32)$$

Note that $\partial(r_3(\tilde{\mathbf{F}}^k) + r_4(\tilde{\mathbf{F}}^k)) \neq \partial r_3(\tilde{\mathbf{F}}^k) + \partial r_4(\tilde{\mathbf{F}}^k)$ for general non-differentiable functions. On account of r_3 and r_4 consisting of l_0 -norm in this paper, we give the above new rule of the separability of the subdifferential. Moreover, the equivalence between the KKT points and the local points is established as follows.

Theorem 1: 1) If $(\tilde{\mathbf{U}}, \tilde{\mathbf{E}}, \tilde{\mathbf{F}})$ is a local minimizer of (30), then it is also a KKT point of (30).

2) If $(\tilde{\mathbf{U}}, \tilde{\mathbf{E}}, \tilde{\mathbf{F}})$ is a KKT point of (30), then there exists a neighborhood $N((\tilde{\mathbf{U}}, \tilde{\mathbf{E}}, \tilde{\mathbf{F}}), \delta)$ such that $(\tilde{\mathbf{U}}, \tilde{\mathbf{E}}, \tilde{\mathbf{F}})$ is a local minimizer of (30), where

$$\delta = \begin{cases} \min \left\{ \min_{(i,j) \in \text{supp}(\tilde{\mathbf{F}})} \sqrt{\delta_2} |\tilde{\mathbf{F}}_{ij}|, \delta_1, \frac{\beta\theta}{c} \right\}, & \tilde{\mathbf{F}} \neq 0, \\ \min \left\{ \delta_1, \frac{\beta\theta}{c} \right\}, & \tilde{\mathbf{F}} = 0, \end{cases} \quad (33)$$

$\delta_1 > 0$, $c > 0$, $\delta_2 = |\text{supp}(\tilde{\mathbf{F}})|$, $\text{supp}(\tilde{\mathbf{F}})$ is the index set of nonzero elements in $\mathbf{F}_{\cdot j}^k$, and $|\text{supp}(\mathbf{F}_{\cdot j}^k)|$ is the cardinality of the set $\text{supp}(\tilde{\mathbf{F}})$.

For ease of reading, the detailed proof of Theorem 1 can be found in the Appendix. Note that the proof of how the two subdifferentials are separable in Definition 1 can also be found in the above proof.

B. Convergence Analysis

Before establishing the global convergence, define

$$\begin{aligned} \mathbf{A}_1 &= \text{Diag}(\mathbf{I}, \mathbf{D}), \mathbf{A}_2 = \text{Diag}(\mathbf{I}, -\mathbf{I}), \\ \mathbf{B}_1 &= \text{Diag}(\mathbf{U}^\tau, \mathbf{U}, \mathbf{U}, \mathbf{U}), \mathbf{B}_2 = \text{Diag}(\mathbf{V}^\tau, \mathbf{F}, \bar{\mathbf{F}}, \mathbf{E}), \\ \mathbf{C} &= \text{Diag}(\mathbf{X}^\tau, \bar{\mathbf{X}}, \bar{\mathbf{X}}, 0), f_1(\bar{\mathbf{B}}_1^\tau) = L_\tau(\mathbf{U}^\tau), \\ f_2(\mathbf{B}_2) &= q(\mathbf{V}^\tau) + r_1(\mathbf{F}) + r_2(\bar{\mathbf{F}}) + p(\mathbf{E}). \end{aligned} \quad (34)$$

Then, problem (9) can be restated as

$$\begin{aligned} \min_{\mathbf{B}_1, \mathbf{B}_2} \quad & f_1(\bar{\mathbf{B}}_1^\tau) + f_2(\mathbf{B}_2) \\ \text{s.t.} \quad & \mathbf{A}_1 \mathbf{B}_1 + \mathbf{A}_2 \mathbf{B}_2 = \mathbf{C}, \end{aligned} \quad (35)$$

where $f_1(\bar{\mathbf{B}}_1^\tau)$ is continuously differentiable and convex and $f_2(\mathbf{B}_2)$ is proper and lower semi-continuous.

Note that $p(\mathbf{E})$ is indivisible with respect to \mathbf{E}^k , $k \in [K]$, so the constraints in (35) are necessary. Naturally, the augmented Lagrangian function of (35) is

$$\begin{aligned} \mathcal{L}_\sigma(\tilde{\mathbf{Y}}) &= f_1(\bar{\mathbf{B}}_1^\tau) + f_2(\mathbf{B}_2) - \frac{1}{2\sigma} \|\mathbf{\Lambda}\|_F^2 \\ &\quad + \frac{\sigma}{2} \|\mathbf{A}_1 \mathbf{B}_1 + \mathbf{A}_2 \mathbf{B}_2 - \mathbf{C} + \frac{1}{\sigma} \mathbf{\Lambda}\|_F^2 \\ &= \mathcal{L}_\sigma(\Upsilon_1, \mathbf{U}; \Upsilon_2), \end{aligned} \quad (36)$$

where $\tilde{\mathbf{Y}} = (\mathbf{B}_2, \mathbf{B}_1, \mathbf{\Lambda})$ and $\mathbf{\Lambda} = \text{Diag}(\mathbf{Q}^\tau, \mathbf{G}, \bar{\mathbf{G}}, \mathbf{H})$.

For (35), we adopt the 2-block proximal ADMM to iteratively update both the original variables \mathbf{B}_2 and \mathbf{B}_1 , and the dual variable $\mathbf{\Lambda}$. Firstly, we construct a potential function as

$$\hat{\mathcal{L}}_\sigma(\tilde{\mathbf{Y}}, \bar{\mathbf{U}}^{\bar{\tau}}) = \mathcal{L}_\sigma(\tilde{\mathbf{Y}}) + \frac{2\gamma^2}{\sigma} \|\mathbf{U}^{\bar{\tau}} - \bar{\mathbf{U}}^{\bar{\tau}}\|_F^2. \quad (37)$$

Next, we give some necessary assumptions for convergence analysis below.

Assumption 1: $L_\tau(\cdot)$ is gradient Lipschitz continuous with a constant $l_u > 0$, that is,

$$\|\nabla L_\tau(\mathbf{U}_1^\tau) - \nabla L_\tau(\mathbf{U}_2^\tau)\|_F \leq l_u \|\mathbf{U}_1^\tau - \mathbf{U}_2^\tau\|_F \quad (38)$$

for any \mathbf{U}_1^τ and \mathbf{U}_2^τ in the feasible region.

Assumption 2: σ satisfies that $\sigma > \max\{\frac{\sqrt{6}}{3}l_u, \sqrt{2}\gamma\}$.

Assumption 3: $\text{Im}(\mathbf{A}_1) \supset \text{Im}(\mathbf{A}_2) \cup \{\mathbf{C}\}$ for $\tilde{\mathbf{Y}}^{(t+1)}$.

Assumption 4: $f(\mathbf{Y}_1, \mathbf{U}) := L_\tau(\mathbf{U}^\tau) + q(\mathbf{V}^{\bar{\tau}}) + p(\mathbf{E}) + r_1(\mathbf{F}) + r_2(\bar{\mathbf{F}})$ is coercive².

Remark 1: Assumptions 1-4 are quite prevalent in proving convergence [41], [42]. Assumption 1 is usually used to control the gradient change of the function, which helps to derive the decrease of $\hat{\mathcal{L}}_\sigma(\tilde{\mathbf{Y}}, \bar{\mathbf{U}}^{\bar{\tau}})$ in each iteration, and then prove the convergence of Algorithm 1. Additionally, it contributes to ensuring that neither gradient explosion nor gradient vanishing occurs during the iteration process, thus guaranteeing the stability of Algorithm 1. Assumption 2 ensures the descent property of the function $\hat{\mathcal{L}}_\sigma$. Since positive constants l_u and γ can be very small, it is easy to find a suitable σ . Compared with [41], [42], we remove the assumption that \mathbf{A}_1 has full row rank, so the inclusion relation of Assumption 3 only needs to hold at $\tilde{\mathbf{Y}}^{(t+1)}$ instead of the entire feasible region. The sparsity of matrices $\mathbf{E}^{(t+1)}$, $\mathbf{F}^{(t+1)}$, and $\bar{\mathbf{F}}^{(t+1)}$ makes Assumption 3 naturally satisfied. Assumption 3 not only makes the equality constraint in (9) and (35) hold but also plays a crucial role in the relationship between the decrease of the multiplier and that of the variable. Assumption 4 guarantees the boundedness of the iterative sequence, because $f(\mathbf{Y}_1, \mathbf{U})$ is coercive implying that it is bounded from below.

Further, we will give the descent property of the potential function and the boundedness of variables that allows the convergence of $\{\hat{\mathcal{L}}_\sigma(\tilde{\mathbf{Y}}^{(t)}, \mathbf{U}^{\bar{\tau}(t-1)})\}$ and the vanishing of $\|\mathbf{Y}^{(t+1)} - \mathbf{Y}^{(t)}\|_F$, where $\mathbf{Y}^{(t+1)} = (\mathbf{Y}_1^{(t+1)}, \mathbf{U}^{(t+1)}; \mathbf{Y}_2^{(t+1)})$.

Lemma 1: Let $\{\mathbf{Y}^{(t)}\}_{t=1}^\infty$ be the sequence generated by Algorithm 1. If Assumptions 1-3 hold, then

- 1) $\hat{\mathcal{L}}_\sigma(\tilde{\mathbf{Y}}^{(t+1)}, \mathbf{U}^{\bar{\tau}(t)}) < \hat{\mathcal{L}}_\sigma(\tilde{\mathbf{Y}}^{(t)}, \mathbf{U}^{\bar{\tau}(t-1)})$;
- 2) $d(0, \partial \hat{\mathcal{L}}_\sigma(\tilde{\mathbf{Y}}^{(t)}, \mathbf{U}^{\bar{\tau}(t-1)})) \leq \tilde{w}(\|\mathbf{U}^{(t)} - \mathbf{U}^{(t-1)}\|_F + \|\mathbf{U}^{(t-1)} - \mathbf{U}^{(t-2)}\|_F)$, where $\tilde{w} = \sqrt{2\sigma + \lambda_{\max}(\mathbf{D}^\top \mathbf{D})} + \max\{\sqrt{2\sigma} + \frac{4\sqrt{2}\gamma^2 + \sqrt{2}\gamma}{\sigma} + (2\sqrt{2} + \sqrt{2\lambda_{\max}(\mathbf{D}^\top \mathbf{D})})\gamma, \sqrt{2}l_u + \frac{\sqrt{2}l_u}{\sigma} + \sqrt{2\lambda_{\max}(\mathbf{D}^\top \mathbf{D})}l_u\}$.

By Lemma 1, the descent property of function $\hat{\mathcal{L}}_\sigma(\tilde{\mathbf{Y}}^{(t+1)}, \mathbf{U}^{\bar{\tau}(t)})$ and the boundedness for its subgradient are given, which makes further preparation for proving the convergence of sequence $\{\mathbf{Y}^{(t)}\}$.

Lemma 2: Under Assumptions 1-4, the following results hold.

- 1) The sequence $\{\mathbf{Y}^{(t)}\}_{t=1}^\infty$ is bounded;
- 2) $\|\mathbf{Y}^{(t+1)} - \mathbf{Y}^{(t)}\|_F \rightarrow 0$ as $t \rightarrow +\infty$.

From [43], it is evident that $\hat{\mathcal{L}}_\sigma(\cdot, \cdot)$ is a KL function, thus the global convergence of the sequence $\{\mathbf{Y}^{(t)}\}_{t=1}^{+\infty}$ can be established.

Theorem 2: Suppose that Assumptions 1-4 are also satisfied. Then, the following hold:

- 1) Any accumulation point $\tilde{\mathbf{Y}}$ of the generated sequence $\{\mathbf{Y}^{(t)}\}_{t=1}^{+\infty}$ is a KKT point of (30);
- 2) Because $\hat{\mathcal{L}}_\sigma(\cdot, \cdot)$ is a KL function, the sequence $\{\mathbf{Y}^{(t)}\}_{t=1}^{+\infty}$ converges to a KKT point of (30).

For the interested readers, please go to the Appendix for the detailed proofs of the above theoretical results.

²Function $f(\mathbf{A})$ is said to be coercive if $f(\mathbf{A}) \rightarrow +\infty$ when $\|\mathbf{A}\|_F \rightarrow +\infty$.

V. NUMERICAL EXPERIMENTS

In this section, we compare state-of-the-art multi-view clustering methods to evaluate the performance of our proposed method. To measure the accuracy of clustering, four indicators are chosen, including adjusted Rand index (ARI) [44], F-score [45], false negative rate (FNR), and false positive rate (FPR). The higher the ARI and F-score, the smaller the FNR and FPR, and the better the clustering performance.

A. Simulation Studies

In this subsection, the proposed method will be compared with SCC [32], iGecco+ [23], K -means clustering (K -means), and Hierarchical clustering (Hclust). SCC and iGecco+ are the sparse convex clustering techniques with inter-group Lasso penalty in (4) and (5). K -means and Hclust are baseline methods whose experimental results are obtained by executing the built-in functions `kmeans` and `clusterdata` in MATLAB, respectively. Except for the baseline methods, the rest are fusion regularized clustering.

We consider the following four simulation scenarios with semi-spherical shells [31] and with spheres [23], where each simulated data consists of $n = 120$ observations, with $K = 3$ clusters, and the number of observations in each cluster is equal. Specifically speaking,

- S1: Count data. The first 3 features are informative and are generated from Poisson distributions with different λ_k ($k = 1, 2, 3$) for each class. Specifically, $\lambda_1 = 1e_3$, $\lambda_2 = 2e_3$, $\lambda_3 = 3e_3$. The remaining features (i.e., noise) follow a Poisson distribution with the identical and randomly generated λ ($\lambda \in \{1, 2, 3, \dots, 10\}$). The number of noise features changes from 0 to 250 in increments of 50.
- S2: Binary data. The first 3 features are informative and are generated from Bernoulli distributions with different λ_k ($\lambda_1 = 0.1e_3$, $\lambda_2 = 0.2e_3$, $\lambda_3 = 0.3e_3$) for each class. The remaining features (i.e., noise) follow a Bernoulli distribution with the identical and randomly generated λ ($\lambda \in \{0.1, 0.2, 0.3, \dots, 0.9\}$). The number of noise features varies from 0 to 250 in increments of 50.
- S3: Mixed data with $p_1 > p_2 > p_3$. The first 10 features of each view are valid features, which obey the Gaussian distribution, Poisson distribution, and Bernoulli distribution respectively. For each class, the Gaussian data is generated from $N(\lambda_k, v_k e_{10})$ ($\lambda_1 = [2.5e_5^\top \ 2e_5^\top]^\top$, $\lambda_2 = 2e_{10}$, $\lambda_3 = 2.5e_{10}$, $v_1 = 2$, $v_2 = 2.5$, $v_3 = 2$), the count data is generated from Poisson with different λ_k ($\lambda_1 = 7e_{10}$, $\lambda_2 = 9e_{10}$, $\lambda_3 = 8e_{10}$), and the binary data is generated from Bernoulli with different λ_k ($\lambda_1 = 0.1e_{10}$, $\lambda_2 = 0.2e_{10}$, $\lambda_3 = 0.15e_{10}$). Additionally, the noise features of the counterpart view also follow the same distribution. In each class, the Gaussian noise follow $N(0, 1)$, whose number ranges from 190, 390, 790, 1590 to 2290, the Poisson noise have the same integer λ within the range of [1, 10], and its number changes from 90, 190, 440, 890 to 1090, and the Bernoulli noise have the same λ ($\lambda \in \{0.1, 0.2, 0.3, \dots, 0.9\}$), and its number changes from 40, 90, 240, 490 to 590.

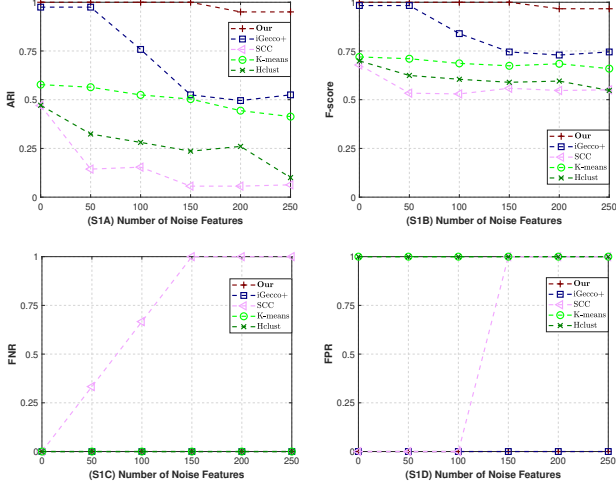


Fig. 1. Simulation results of different clustering methods on the count data S1 under varying number of noise features: (S1A) ARI, (S1B) F-score, (S1C) FNR, (S1D) FPR.

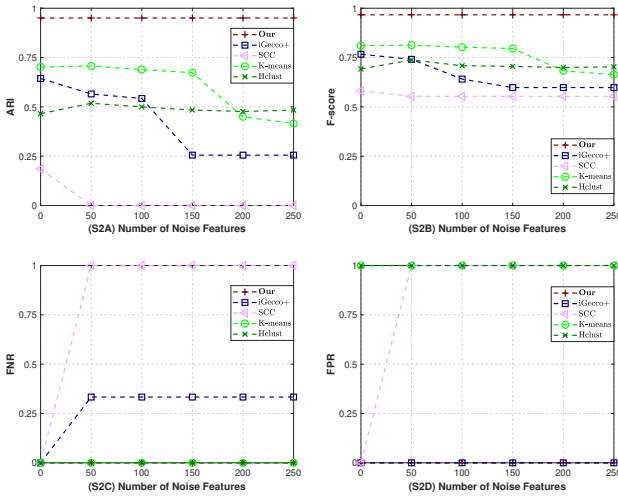


Fig. 2. Simulation results of different clustering methods on the binary data S2 under varying number of noise features: (S2A) ARI, (S2B) F-score, (S2C) FNR, (S2D) FPR.

- S4: Mixed data with $p_2 > p_3 > p_1$. The data is generated similarly to S3, with the only difference being the amount of Gaussian noise, Poisson noise, and Bernoulli noise. Specifically, the Gaussian noise changes from 40, 90, 240, 490 to 590, the Poisson noise changes from 190, 390, 790, 1590 to 2290, and Bernoulli noise changes from 90, 190, 440, 890 to 1090.

For better fitting, we respectively apply the Euclidean distance, the Manhattan distance, and the Bernoulli log-likelihood to Gaussian data, count data, and binary data, because these metrics are superior to other loss functions and offer faster computation speeds. Simultaneously, we employ the adaptive parameter adjustment method described in [23] to adjust parameters ζ_k , η , w_l , β , and $\bar{\beta}^k$, and adopt the grid search method to select θ from $\{2^{-10}, 2^{-9}, 2^{-8}, \dots, 2^0\}$. To be fair, all fusion regularized clustering methods are resolved by

TABLE II
SIMULATION RESULTS OF DIFFERENT CLUSTERING METHODS ON THE MIXED DATA S3.

p (p_1, p_2, p_3)	Method	ARI \uparrow	F-score \uparrow	FNR \downarrow	FPR \downarrow
350 (200, 100, 50)	iGecco+ Our	1.0000 1.0000	1.0000 1.0000	0.0000 0.0000	0.0645 0.0000
700 (400, 200, 100)	iGecco+ Our	1.0000 1.0000	1.0000 1.0000	0.0000 0.0000	0.0645 0.0000
1500 (800, 450, 250)	iGecco+ Our	0.9337 1.0000	0.9337 1.0000	0.0000 0.0000	0.9670 0.0000
3000 (1600, 900, 500)	iGecco+ Our	0.8340 1.0000	0.8946 1.0000	0.2333 0.0000	0.9446 0.0625
4000 (2300, 1100, 600)	iGecco+ Our	0.6395 1.0000	0.8295 1.0000	0.0000 0.0000	0.9148 0.1429

TABLE III
SIMULATION RESULTS OF DIFFERENT CLUSTERING METHODS ON THE MIXED DATA S4.

p (p_1, p_2, p_3)	Method	ARI \uparrow	F-score \uparrow	FNR \downarrow	FPR \downarrow
350 (50, 200, 100)	iGecco+ Our	1.0000 1.0000	1.0000 1.0000	0.0000 0.0000	0.6703 0.0000
700 (100, 400, 200)	iGecco+ Our	0.8337 1.0000	0.8918 1.0000	0.0333 0.0000	0.4200 0.0000
1500 (250, 800, 450)	iGecco+ Our	0.8139 1.0000	0.8622 1.0000	0.1000 0.0000	0.4672 0.0000
3000 (500, 1600, 900)	iGecco+ Our	0.7576 1.0000	0.8468 1.0000	0.2333 0.0000	0.7534 0.0000
4000 (600, 2300, 1100)	iGecco+ Our	0.7223 1.0000	0.8287 1.0000	0.2667 0.0000	0.6765 0.0208

ADMM, and they use the same method to select parameters.

Figs. 1 and 2 exhibit that our method has the best clustering performance and feature selection ability, and still outperforms others as the amount of noise increases. Both our method and iGecco+ can correctly select effective features in S1, however, it is interesting that our method is superior to iGecco+, which indicates that the group sparsity can eliminate some unnecessary data points. The randomly generated effective features inevitably contain samples around the cluster dividing line, which are not helpful to clustering or even unfavorable to clustering. In S2, the FNR of iGecco+ increases, that is, some effective features are filtered out, which implies that l_0 -norm has a certain advantage over l_1 -norm in high dimensions. As shown in (S1C), (S1D), (S2C), and (S2D), the error rate of feature selection for SCC without the influence of \bar{x} is higher than that for our method and iGecco+ with the influence of \bar{x} taken into account, where $\bar{x} \neq 0$ in S1 and S2. The FNR=0 and FPR=1 of both K-means and Hclust reflect that neither method has the capability of feature selection, so that all features are considered to be valid features.

Tables II and III list the results of S3 and S4. It is found that our designed method performs better than iGecco+, especially in high dimensions. Note that compared with S1 and S2, we reduce the differences in the cluster mean centroids λ_k of the informative features on binary and count data in S3 and S4 to reduce the disparities among various clusters.

B. Real-data Examples

In this subsection, we apply three common data listed in Table IV to evaluate our proposed method.

TABLE IV
DETAILS OF REAL DATA.

Data	Views	Observations	Features	Clusters	Points of per cluster
Authors	1	841	69	4	317, 296, 55, 173
Lung-discrete	1	73	325	7	6, 5, 5, 16, 7, 13, 21
MSRCV1	6	210	2428	7	30, 30, 30, 30, 30, 30, 30

TABLE V
COMPARISONS OF ARI AND F-SCORE FOR DIFFERENT CLUSTERING METHODS ON THE REAL DATA.

Data	Methods	K-means	Hclust	COMVSC	SCMvFS	SCC	SGLCC	iGecco+	Our
Authors	ARI	0.7276	0.7461	0.8536	0.7985	0.8941	0.8941	0.9698	0.9929
	F-score	0.8089	0.8223	0.8986	0.8595	0.9291	0.9291	0.9792	0.9951
Lung-discrete	ARI	0.5039	0.4394	0.5608	0.5714	0.5516	0.6665	0.5516	0.7345
	F-score	0.5953	0.5372	0.5680	0.6479	0.6668	0.7251	0.6668	0.7809
MSRCV1	ARI	0.4639	0.3903	0.4586	0.4667	0.4466	0.0816	0.5853	0.6684
	F-score	0.5503	0.5088	0.6198	0.5557	0.5707	0.3777	0.6723	0.7305

TABLE VI
ABLATION STUDY OF CLUSTERING PERFORMANCE AND FEATURE SELECTION CAPABILITY.

Data	$\ \cdot\ _{2,0}$	$\ \cdot\ _0$	ARI \uparrow	F-score \uparrow	$ T_{now} \cap T_{our} $	Selected feature number
Authors	✓	✓	0.9960	0.9972	3	3
	×	✓	0.6741	0.8122	3	9
	✓	×	0.9929	0.9951	3	4
	×	×	0.9887	0.9922	3	69
Lung-discrete	✓	✓	0.7345	0.7809	73	73
	×	✓	0.6912	0.7460	47	161
	✓	×	0.6368	0.7086	27	68
	×	×	0.5587	0.6639	73	325
MSRCV1	✓	✓	0.6684	0.7305	175	175
	×	✓	0.4907	0.6145	170	1098
	✓	×	0.4904	0.6131	138	1068
	×	×	0.3496	0.5411	175	2428

- Authors³ is composed of word counts from 841 chapters written by four famous English-language authors (Austen, London, Milton, and Shakespeare). Each class includes an unbalanced number of observations with 69 features.
- Lung-discrete⁴ is a biological data which contains 73 observations with 325 features, and each sample belongs to one of 7 classes.
- MSRCV1⁵ is an image data containing 210 images with 7 classes: tree, car, face, cow, bicycle, building, and airplane. The features of these images are collected from 6 views: Census Transform (CENT), CMT, Generalized Search Tree, HOG, LBP, and Scale Invariant Feature Transform. We take the log of CENT and take the square root of LBP and HOG. Further, we use the Z-score method to standardize the entire data.

To highlight the merits of our proposed method, we conduct a series of methodological comparisons. Compared with the experiment of simulated data, three methods are added here:

- SGLCC [33]: Convex fusion regularized clustering with group Lasso penalty.
- COMVSC [46]: Consensus one-step multi-view subspace clustering, which integrates representation learning, partition fusion, and clustering into a unified framework.

- SCMvFS [47]: Structure learning with consensus label information and heterogeneous graphs for multi-view feature selection.

Again, the baseline methods are K -means and Hclust. To be fair, we use the same way of parameter selection and solution on unsupervised fusion regularization methods, including SCC, SGLCC, iGecco+, and our method. In addition, according to the distribution of the real single-view data shown in Fig. 3, we select appropriate loss functions, which are Manhattan distance and Euclidean distance respectively.

As can be seen from Table V, when $\bar{x} \neq 0$, SGLCC can achieve the highest accuracy only when it degenerates into SCC. This is attributable to the fact that both the selected features and the chosen data points may be erroneous. When $\bar{x} = 0$, iGecco+ is equivalent to SCC so that they have the same accuracy. We observe that our method has the highest clustering accuracy. In comparison with the other two multi-view clustering methods, namely COMVSC and SCMvFS, the average ARI of our method is enhanced by 15.65% and 17.87%, respectively. When compared with the three fusion regularized clustering methods (SCC, SGLCC, and iGecco+), our method increases the average ARI by approximately 14.08%, 8.34%, and 10.30%, respectively.

On the other hand, our approach also performs well for the multi-view data MSRCV1. The reason for the poor clustering effect of SCC and SGLCC is that they do not take into account the disparity of 6-view data. Instead, they uniformly

³<https://github.com/DataSlings/clustRviz/tree/master/data>

⁴<https://jundongl.github.io/scikit-feature/datasets.html>

⁵<https://github.com/Jeaninezpp/multi-view-datasets>

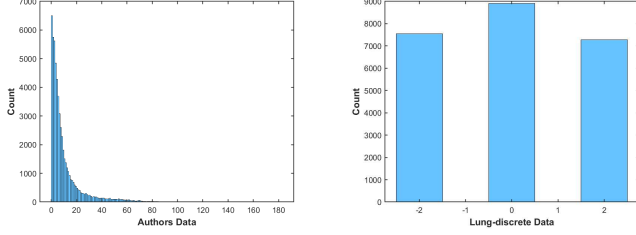


Fig. 3. Histograms of Authors and Lung-discrete. Authors is highly-skewed, and Lung-discrete appears discrete Gaussian.

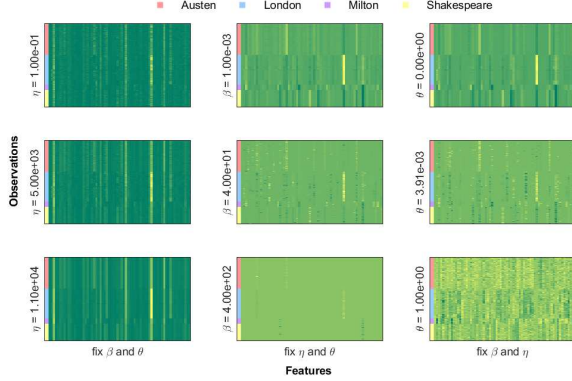


Fig. 4. Clustering path η and regularization path β , θ of our method for Authors. From left to right, we characterize the responses of \tilde{U} by fixing β and θ and adjusting η , the responses of $\tilde{U} - \tilde{X}$ by fixing η and θ and adjusting β , and the responses of $\tilde{U} - \tilde{X}$ by fixing β and η and adjusting θ , respectively.

treat all data as single-view data following a standard normal distribution. Besides, since the group sparsity of SGLCC does not centralize the centroid matrix in advance, its performance is worse compared to SCC with inter-group sparsity that also does not undergo the centralization process. Similarly, in contrast to COMVSC, SCMvFS, SCC, and iGecco+, our method increases ARI by about 20.98%, 20.17%, 22.18%, and 8.31%, respectively.

C. Discussions

1) *Ablation Study*: To further illustrate the effectiveness of the group sparsity strategy, we carry out sufficient ablation experiments. As shown in Table VI, it is evident that our clustering approach is superior to the other three clustering methods. Specifically, for Authors, Lung-discrete, and MSRCV1, when merely the inter-group sparsity term $\|\cdot\|_{2,0}$ and the intra-group sparsity term $\|\cdot\|_0$ are incorporated, some redundant features may be mistaken for significant ones, leading to inferior clustering performance compared to our scheme. When neither module is added, all features will be considered important. In this case, the performance of clustering methods without feature selection capability deteriorates further as the number of features increases, which may be associated with growth in the number of noise features.

Let T_{now} and T_{our} denote the feature sets selected by the current clustering method and our clustering method, respectively. $|T_{now} \cap T_{our}|$ represents the cardinality of the

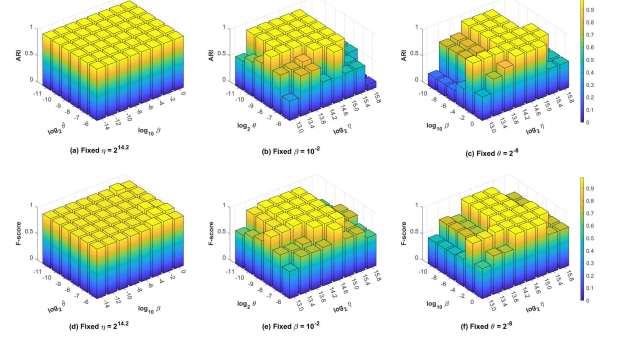


Fig. 5. Parameter sensitivity using ARI and F-score.

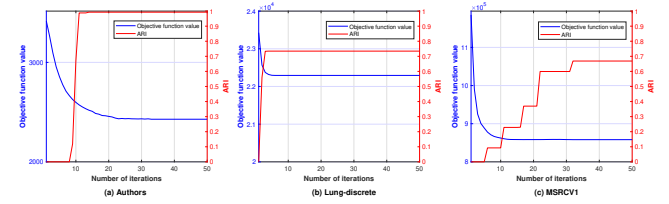


Fig. 6. Objective function value and ARI versus the iteration of our method on (a) Authors, (b) Lung-discrete, and (c) MSRCV1.

intersection of two sets T_{now} and T_{our} . From Table VI, the total number of features selected by only considering $\|\cdot\|_{2,0}$ or $\|\cdot\|_0$ is inconsistent with that by our method. In particular, for Lung-discrete and MSRCV1, the feature sets selected by these two methods both satisfy $|T_{now} \cap T_{our}| < |T_{our}|$. All of the above indications suggest that the omission of informative features can also affect the clustering results. In summary, different components $\|\cdot\|_{2,0}$ and $\|\cdot\|_0$ play certain roles in feature selection and clustering accuracy, and our model with group sparsity has a distinct advantage.

2) *Parameter Analysis*: We perform sensitivity analysis of the tuning parameters η , β , and θ by applying our method on Authors. Fig. 4 reflects how \tilde{U} and $\tilde{U} - \tilde{X}$ change as a function of three tuning parameters, where the size of \tilde{U} and $\tilde{U} - \tilde{X}$ can clearly describe the situation of clustering and feature selection respectively. It is found that

- If we fix β and θ , the number of clusters decreases as the increase of η .
- If we fix η and θ , the number of selected features decreases with the increase of β .
- Fixing β and η , when $\theta = 0$, whole informative features are selected. As θ increases, local informative features are selected. Until $\theta = 1$, the model does not have feature selection capability because all features are selected.

In addition, Fig. 5 shows the 3-D histograms of the change in ARI and F-score. It can be observed that when η is fixed, the ARI and F-score are not sensitive to changes in the penalty parameters θ and β . When β or θ is fixed, our proposed method maintains good performance over a wide range.

3) *Convergence*: Fig. 6 shows the objective function value $f(\Upsilon_1, U)$ and ARI versus the number of iterations under Authors, Lung-discrete, and MSRCV1. From the figure, it is

evident that the objective function value decreases as the number of iterations increases, while the ARI exhibits an overall increasing trend with respect to the number of iterations, and both eventually converge to a constant value.

VI. CONCLUSIONS

In this paper, we propose a novel multi-view fusion regularized clustering method to address *mixed types* and *high dimensionality* in high-dimensional mixed settings. To the best of our knowledge, this is the first time that non-convex group sparsity is introduced into fusion regularized clustering methods. Extensive experimental results verify its advantages, especially on the MSRCV1 dataset, where the proposed method improves ARI by at least 8.31% and F-score by at least 5.82% over the existing methods. In addition, for the proposed non-convex non-smooth model, we develop an efficient proximal ADMM algorithm. By utilizing spatial decomposition techniques, we derive the equivalence between local minima and KKT points in a specific region. Furthermore, under mild conditions, we establish global convergence without considering existing approximation or smoothing methods, which is of great importance theoretically.

In future work, we are interested in achieving a certain degree of privacy protection for data while clustering. Besides, combining clustering with deep learning to improve representation performance is also a potential direction.

APPENDIX

PROOF OF THEOREM 1

Proof: 1) Due to $(\tilde{U}, \tilde{E}, \tilde{F})$ is a local minimizer for problem (30), \tilde{U} , \tilde{E} , and \tilde{F}^k are respectively the local minimizers of the following problems

$$\begin{aligned} \min_{\mathbf{U}} \quad & L_\tau(\mathbf{U}^\tau) + L_{\tilde{\tau}}(\mathbf{U}^{\tilde{\tau}}) \\ \text{s.t.} \quad & \mathbf{DU} = \tilde{\mathbf{E}}, \quad \mathbf{U} - \tilde{\mathbf{X}} = \tilde{\mathbf{F}}, \end{aligned} \quad (39)$$

$$\begin{aligned} \min_{\mathbf{E}} \quad & p(\mathbf{E}) \\ \text{s.t.} \quad & \mathbf{D}\tilde{\mathbf{U}} = \mathbf{E}, \end{aligned} \quad (40)$$

and

$$\begin{aligned} \min_{\mathbf{F}^k} \quad & r_3(\mathbf{F}^k) + r_4(\mathbf{F}^k) \\ \text{s.t.} \quad & \tilde{\mathbf{U}}^k - \tilde{\mathbf{X}}^k = \mathbf{F}^k, k \in [K]. \end{aligned} \quad (41)$$

According to [48, Theorem 2.1], we can get that $\tilde{\mathbf{U}}$ is a KKT point for (39). Obviously, it follows from the subdifferential chain rule in [49, Corollary 2.52] that $\tilde{\mathbf{E}}$ is a KKT point for (40).

Define

$$\begin{aligned} I_1^k &:= \{j \mid \|\mathbf{F}_{\cdot j}^k\|_2 \neq 0, |\text{supp}(\mathbf{F}_{\cdot j}^k)| = n\}, \\ I_2^k &:= \{j \mid \|\mathbf{F}_{\cdot j}^k\|_2 \neq 0, |\text{supp}(\mathbf{F}_{\cdot j}^k)| < n\}, \\ I_3^k &:= \{j \mid \|\mathbf{F}_{\cdot j}^k\|_2 = 0\}, \end{aligned} \quad (42)$$

where $\text{supp}(\mathbf{F}_{\cdot j}^k)$ is the index set of nonzero elements in $\mathbf{F}_{\cdot j}^k$, and $|\text{supp}(\mathbf{F}_{\cdot j}^k)|$ is the cardinality for the set $\text{supp}(\mathbf{F}_{\cdot j}^k)$.

For the \mathbf{F}^k -problem (41), on account of $r_3(\mathbf{F}^k) = \sum_{j=1}^{p_k} \beta(1-\theta)\mathbb{I}(\beta_j^k \|\mathbf{F}_{\cdot j}^k\|_2 \neq 0) = \sum_{j=1}^{p_k} \beta(1-\theta)\mathbb{I}(\|\mathbf{F}_{\cdot j}^k\|_2 \neq$

0) and $r_4(\mathbf{F}^k) = \sum_{j=1}^{p_k} \beta\theta\|\mathbf{F}_{\cdot j}^k\|_0 = \sum_{i=1}^n \sum_{j=1}^{p_k} \beta\theta\mathbb{I}(\mathbf{F}_{ij}^k \neq 0)$, it follows from [50, Proposition 10.5] that the limiting subdifferentials can be separated that for $s = 3, 4$,

$$\partial r_s(\tilde{\mathbf{F}}^k) = \partial r_s(\tilde{\mathbf{F}}_1^k) \times \partial r_s(\tilde{\mathbf{F}}_2^k) \times \cdots \times \partial r_s(\tilde{\mathbf{F}}_{p_k}^k), \quad (43)$$

and hence $\partial r_s(\tilde{\mathbf{F}}^k) = \partial r_s(\tilde{\mathbf{F}}_{I_1^k}^k) \times \partial r_s(\tilde{\mathbf{F}}_{I_2^k}^k) \times \partial r_s(\tilde{\mathbf{F}}_{I_3^k}^k)$, $s = 3, 4$.

Next, we analyze the properties of these three partitioned matrices: $\tilde{\mathbf{F}}_{I_1^k}^k$, $\tilde{\mathbf{F}}_{I_2^k}^k$, and $\tilde{\mathbf{F}}_{I_3^k}^k$. Let \bar{I}_a^k be the complement of I_a^k with respect to $\{1, 2, \dots, p_k\}$, $a = 1, 2, 3$. Observe that $\tilde{\mathbf{F}}_{I_a^k}^k$ is a local minimizer of the restricted problem

$$\begin{aligned} \min_{\mathbf{F}_{I_a^k}^k} \quad & r_3(\mathbf{F}_{I_a^k}^k, \tilde{\mathbf{F}}_{\bar{I}_a^k}^k) + r_4(\mathbf{F}_{I_a^k}^k, \tilde{\mathbf{F}}_{\bar{I}_a^k}^k) \\ \text{s.t.} \quad & [\tilde{\mathbf{U}}_{I_a^k}^k \quad \tilde{\mathbf{U}}_{\bar{I}_a^k}^k] - [\tilde{\mathbf{X}}_{I_a^k}^k \quad \tilde{\mathbf{X}}_{\bar{I}_a^k}^k] = [\mathbf{F}_{I_a^k}^k \quad \tilde{\mathbf{F}}_{\bar{I}_a^k}^k]. \end{aligned} \quad (44)$$

For all $j \in I_1^k$, $r_3(\mathbf{F}_j^k)$ and $r_4(\mathbf{F}_j^k)$ are strictly differentiable, and BQ holds at $\tilde{\mathbf{F}}_{I_1^k}^k$ for (44) in accordance with [48]. Thus, $\tilde{\mathbf{F}}_{I_1^k}^k$ is a KKT point of problem (44) when $a = 1$.

For all $j \in I_2^k$, $r_3(\mathbf{F}_j^k)$ is strictly differentiable, we know that $\partial r_3(\tilde{\mathbf{F}}_j^k) = \partial^\infty r_3(\tilde{\mathbf{F}}_j^k) = \{0\}$, and $\partial^\infty r_4(\tilde{\mathbf{F}}_j^k) = \{\mathbf{v} \in \mathbb{R}^n \mid \mathbf{v}_i = 0, (i, j) \in \text{supp}(\tilde{\mathbf{F}}^k)\}$. From [50, Exercise 10.10], we have

$$\begin{aligned} \partial \left(r_3(\tilde{\mathbf{F}}_j^k) + r_4(\tilde{\mathbf{F}}_j^k) \right) &= \bar{\beta}_j^k \partial r_3(\tilde{\mathbf{F}}_j^k) + \partial r_4(\tilde{\mathbf{F}}_j^k) \\ &= \partial r_4(\tilde{\mathbf{F}}_j^k), \end{aligned} \quad (45)$$

$$\partial^\infty \left(r_3(\tilde{\mathbf{F}}_j^k) + r_4(\tilde{\mathbf{F}}_j^k) \right) = \partial^\infty r_4(\tilde{\mathbf{F}}_j^k).$$

Based on the separability of matrix $\tilde{\mathbf{F}}_j^k$, we obtain that

$$\partial r_4(\tilde{\mathbf{F}}_j^k) = \partial r_4(\tilde{\mathbf{F}}_{s_1 j}^k) \times \partial r_4(\tilde{\mathbf{F}}_{s_2 j}^k), \quad (46)$$

where $s_1 = \{i \mid i \in \text{supp}(\tilde{\mathbf{F}}_{\cdot j}^k)\}$, $s_2 = \{i \mid i \in \overline{\text{supp}}(\tilde{\mathbf{F}}_{\cdot j}^k)\}$, $\overline{\text{supp}}$ is the complement of supp . Obviously, $0 \in \partial r_4(\tilde{\mathbf{F}}_{s_1 j}^k) - \mathbf{G}_{s_1 j}^k$, $\forall k \in [K]$. Since $\partial r_4(\tilde{\mathbf{F}}_{ij}^k)$ is the whole real line for each $i \in s_2$, the inclusion

$$0 \in \partial r_4(\tilde{\mathbf{F}}_{s_2 j}^k) - \mathbf{G}_{s_2 j}^k, \quad \forall k \in [K] \quad (47)$$

always holds. Therefore, $\tilde{\mathbf{F}}_{I_2^k}^k$ is a KKT point of problem (44) when $a = 2$.

For all $j \in I_3^k$, $\partial r_3(\tilde{\mathbf{F}}_j^k) = \partial r_4(\tilde{\mathbf{F}}_j^k) = \mathbb{R}^n$, we have

$$\partial \left(r_3(\tilde{\mathbf{F}}_j^k) + r_4(\tilde{\mathbf{F}}_j^k) \right) \subset \bar{\beta}_j^k \partial r_3(\tilde{\mathbf{F}}_j^k) + \partial r_4(\tilde{\mathbf{F}}_j^k) = \mathbb{R}^n,$$

that is

$$0 \in \bar{\beta}_j^k \partial r_3(\tilde{\mathbf{F}}_j^k) + \partial r_4(\tilde{\mathbf{F}}_j^k) - \mathbf{G}_j^k, \quad \forall k \in [K] \quad (48)$$

always holds. Therefore, $\tilde{\mathbf{F}}_{I_3^k}^k$ is a KKT point of problem (44) when $a = 3$.

In conclusion, $(\tilde{\mathbf{U}}, \tilde{\mathbf{E}}, \tilde{\mathbf{F}})$ is a KKT point for problem (30).

2) Before getting further conclusions, some symbols are introduced

$$\begin{aligned} C_1 &= \left\{ (\mathbf{U}, \mathbf{E}, \mathbf{F}) : \mathbf{F}_j = 0, \quad \forall j \in \overline{\text{supp}}(\tilde{\mathbf{F}}) \right\}, \\ C_2 &= \left\{ (\mathbf{U}, \mathbf{E}, \mathbf{F}) : \mathbf{F}_{ij} = 0, \quad \forall (i, j) \in \overline{\text{supp}}(\tilde{\mathbf{F}}) \right\}, \\ \Omega_1 &= \{ (\mathbf{U}, \mathbf{E}, \mathbf{F}) \mid \mathbf{DU} = \mathbf{E}, \mathbf{U} - \tilde{\mathbf{X}} = \mathbf{F} \}, \end{aligned} \quad (49)$$

where $\text{supp}(\tilde{\mathbf{F}})$ is the index set of nonzero columns in $\tilde{\mathbf{F}}$, and $\overline{\text{supp}}$ is the complement of supp .

The norm cones of C_1 and C_2 at $(\tilde{\mathbf{U}}, \tilde{\mathbf{E}}, \tilde{\mathbf{F}})$ are respectively

$$\begin{aligned} & \mathcal{N}_{C_1}(\tilde{\mathbf{U}}, \tilde{\mathbf{E}}, \tilde{\mathbf{F}}) \\ &= \{0\} \times \{0\} \times \left\{ \mathbf{V} \mid \mathbf{V}_j = 0, \forall j \in \text{supp}(\tilde{\mathbf{F}}) \right\}, \\ & \mathcal{N}_{C_2}(\tilde{\mathbf{U}}, \tilde{\mathbf{E}}, \tilde{\mathbf{F}}) \end{aligned} \quad (50)$$

$$= \{0\} \times \{0\} \times \left\{ \mathbf{W} \mid \mathbf{W}_{ij} = 0, \forall (i, j) \in \text{supp}(\tilde{\mathbf{F}}) \right\}.$$

Combine with Definition 1, the KKT condition for problem (30) can be rewritten as

$$\begin{aligned} 0 & \in \begin{pmatrix} \partial L(\tilde{\mathbf{U}}) \\ \partial p(\tilde{\mathbf{E}}) \\ \partial r(\tilde{\mathbf{F}}) \end{pmatrix} + \begin{pmatrix} \mathbf{D}^\top \tilde{\mathbf{H}} + \tilde{\mathbf{G}} \\ -\tilde{\mathbf{H}} \\ -\tilde{\mathbf{G}} \end{pmatrix} \\ &= \begin{pmatrix} \partial L(\tilde{\mathbf{U}}) \\ \partial P(\tilde{\mathbf{E}}) \\ 0 \end{pmatrix} + \mathcal{N}_{C_1}(\tilde{\mathbf{U}}, \tilde{\mathbf{E}}, \tilde{\mathbf{F}}) + \mathcal{N}_{C_2}(\tilde{\mathbf{U}}, \tilde{\mathbf{E}}, \tilde{\mathbf{F}}) \\ & \quad + \mathcal{N}_{\Omega_1}(\tilde{\mathbf{U}}, \tilde{\mathbf{E}}, \tilde{\mathbf{F}}) \end{aligned} \quad (51)$$

where $L(\tilde{\mathbf{U}}) = L_\tau(\tilde{\mathbf{U}}^\tau) + L_{\bar{\tau}}(\tilde{\mathbf{U}}^{\bar{\tau}})$ and $\bar{\beta}$ is a diagonal matrix consisting of K matrices $\bar{\beta}^k$. Further, based on [50, Theorem 6.42], we can obtain that

$$0 \in \begin{pmatrix} \partial L(\tilde{\mathbf{U}}) \\ \partial p(\tilde{\mathbf{E}}) \\ 0 \end{pmatrix} + \mathcal{N}_{C_1 \cap C_2 \cap \Omega_1}(\tilde{\mathbf{U}}, \tilde{\mathbf{E}}, \tilde{\mathbf{F}}). \quad (52)$$

Thus, $(\tilde{\mathbf{U}}, \tilde{\mathbf{E}}, \tilde{\mathbf{F}})$ is a optimal solution of the following convex optimization problem

$$\begin{aligned} & \min_{(\mathbf{U}, \mathbf{E}, \mathbf{F}) \in \Omega_1} L(\mathbf{U}) + p(\mathbf{E}) \\ & \text{s.t.} \quad \mathbf{F}_j = 0, \quad \forall j \in \overline{\text{supp}}(\tilde{\mathbf{F}}), \\ & \quad \mathbf{F}_{ij} = 0, \quad \forall (i, j) \in \overline{\text{supp}}(\tilde{\mathbf{F}}). \end{aligned} \quad (53)$$

Consider a neighborhood:

$$\begin{aligned} N((\tilde{\mathbf{U}}, \tilde{\mathbf{E}}, \tilde{\mathbf{F}}), \delta) &= \left\{ (\mathbf{U}, \mathbf{E}, \mathbf{F}) \mid \|(\mathbf{U}, \mathbf{E}, \mathbf{F}) - (\tilde{\mathbf{U}}, \tilde{\mathbf{E}}, \tilde{\mathbf{F}})\|_F < \delta, \right. \\ & \quad \left. (\tilde{\mathbf{U}}, \tilde{\mathbf{E}}, \tilde{\mathbf{F}}) \in \Omega_1 \right\}, \end{aligned} \quad (54)$$

$$\text{where } \delta = \begin{cases} \min \left\{ \min_{ij \in \text{supp}(\tilde{\mathbf{F}})} \sqrt{\delta_2} |\tilde{\mathbf{F}}_{ij}|, \delta_1, \frac{\beta\theta}{c} \right\}, & \tilde{\mathbf{F}} \neq 0 \\ \min \left\{ \delta_1, \frac{\beta\theta}{c} \right\}, & \tilde{\mathbf{F}} = 0 \end{cases}$$

According to the construction of $N((\tilde{\mathbf{U}}, \tilde{\mathbf{E}}, \tilde{\mathbf{F}}), \delta)$, we have $\|\tilde{\mathbf{F}}\|_{2,0} \leq \|\mathbf{F}\|_{2,0}$ and $\|\tilde{\mathbf{F}}\|_0 \leq \|\mathbf{F}\|_0$ for $\forall (\mathbf{U}, \mathbf{E}, \mathbf{F}) \in N((\tilde{\mathbf{U}}, \tilde{\mathbf{E}}, \tilde{\mathbf{F}}), \delta)$. The following is the proof that $(\tilde{\mathbf{U}}, \tilde{\mathbf{E}}, \tilde{\mathbf{F}})$ is a locally optimal solution of (30) on $N((\tilde{\mathbf{U}}, \tilde{\mathbf{E}}, \tilde{\mathbf{F}}), \delta)$, i.e., for $\forall (\mathbf{U}, \mathbf{E}, \mathbf{F}) \in N((\tilde{\mathbf{U}}, \tilde{\mathbf{E}}, \tilde{\mathbf{F}}), \delta)$,

$$L(\tilde{\mathbf{U}}) + p(\tilde{\mathbf{E}}) + r(\tilde{\mathbf{F}}) \leq L(\mathbf{U}) + p(\mathbf{E}) + r(\mathbf{F}). \quad (55)$$

It follows from the definition of C_1 and C_2 that $C_2 \subseteq C_1$. For $\forall (\mathbf{U}, \mathbf{E}, \mathbf{F}) \in N((\tilde{\mathbf{U}}, \tilde{\mathbf{E}}, \tilde{\mathbf{F}}), \delta)$, we find that

If $(\mathbf{U}, \mathbf{E}, \mathbf{F}) \in C_2$, then $\|\tilde{\mathbf{F}}\|_{2,0} = \|\mathbf{F}\|_{2,0}$ and $\|\tilde{\mathbf{F}}\|_0 = \|\mathbf{F}\|_0$. Therefore, inequality (55) always hold based on (53).

If $(\mathbf{U}, \mathbf{E}, \mathbf{F}) \in C_1 \setminus C_2$, then $\|\tilde{\mathbf{F}}\|_{2,0} = \|\mathbf{F}\|_{2,0}$ and $\|\tilde{\mathbf{F}}\|_0 \leq \|\mathbf{F}\|_0 - 1$. Since $L(\mathbf{U}) + P(\mathbf{E})$ is locally Lipschitz continuous,

there exists a neighbor region $N((\tilde{\mathbf{U}}, \tilde{\mathbf{E}}), \delta_1)$ and a constant $c > 0$ such that

$$|L(\tilde{\mathbf{U}}) + p(\tilde{\mathbf{E}}) - L(\mathbf{U}) - p(\mathbf{E})| \leq c \|(\tilde{\mathbf{U}}, \tilde{\mathbf{E}}) - (\mathbf{U}, \mathbf{E})\|_F. \quad (56)$$

Next, we get

$$\begin{aligned} & L(\tilde{\mathbf{U}}) + p(\tilde{\mathbf{E}}) + r(\tilde{\mathbf{F}}) \\ & \leq L(\mathbf{U}) + p(\mathbf{E}) + c \|(\tilde{\mathbf{U}}, \tilde{\mathbf{E}}) - (\mathbf{U}, \mathbf{E})\|_F + r(\mathbf{F}) - \beta\theta \\ & \leq L(\mathbf{U}) + p(\mathbf{E}) + r(\mathbf{F}). \end{aligned} \quad (57)$$

If $(\mathbf{U}, \mathbf{E}, \mathbf{F}) \notin C_1$, then $\|\tilde{\mathbf{F}}\|_{2,0} \leq \|\mathbf{F}\|_{2,0} - 1$ and $\|\tilde{\mathbf{F}}\|_0 \leq \|\mathbf{F}\|_0 - 1$. Similarly, for $(\mathbf{U}, \mathbf{E}, \mathbf{F}) \in N((\tilde{\mathbf{U}}, \tilde{\mathbf{E}}, \tilde{\mathbf{F}}), \delta)$, it is to obtain

$$\begin{aligned} & L(\tilde{\mathbf{U}}) + p(\tilde{\mathbf{E}}) + r(\tilde{\mathbf{F}}) \\ & \leq L(\mathbf{U}) + p(\mathbf{E}) + c \|(\tilde{\mathbf{U}}, \tilde{\mathbf{E}}) - (\mathbf{U}, \mathbf{E})\|_F + r(\mathbf{F}) - \beta \\ & \leq L(\mathbf{U}) + p(\mathbf{E}) + r(\mathbf{F}). \end{aligned} \quad (58)$$

Therefore, $(\tilde{\mathbf{U}}, \tilde{\mathbf{E}}, \tilde{\mathbf{F}})$ is a local minimizer of problem (30). \blacksquare

THE PROOF OF LEMMA 1

Proof: 1) From (36), it is not hard to observe that $\bar{\mathbf{Y}}^{(t+1)}$ is an optimal solution and the below two equations hold

$$\begin{aligned} \bar{\mathbf{\Lambda}}^{\tau(t+1)} &= \bar{\mathbf{\Lambda}}^{\tau(t)} + \sigma(\bar{\mathbf{A}}_1 \bar{\mathbf{B}}_1^{\tau(t+1)} - \bar{\mathbf{B}}_2^{\tau(t+1)} - \bar{\mathbf{C}}^\tau), \\ \bar{\mathbf{\Lambda}}^{\bar{\tau}(t+1)} &= \bar{\mathbf{\Lambda}}^{\bar{\tau}(t)} + \sigma(\mathbf{A}_1 \mathbf{B}_1^{\bar{\tau}(t+1)} + \mathbf{A}_2 \mathbf{B}_2^{\bar{\tau}(t+1)} - \mathbf{C}^{\bar{\tau}}) \end{aligned} \quad (59)$$

where

$$\begin{aligned} \bar{\mathbf{A}}_1 &= \text{Diag}(\mathbf{I}, \mathbf{D}), \bar{\mathbf{B}}_1^\tau = \text{Diag}(\mathbf{U}^\tau, \mathbf{U}^\tau, \mathbf{U}^\tau), \\ \bar{\mathbf{B}}_2^\tau &= \text{Diag}(\mathbf{F}^\tau, \bar{\mathbf{F}}^\tau, \bar{\mathbf{E}}^\tau), \bar{\mathbf{C}}^\tau = \text{Diag}(\bar{\mathbf{X}}^\tau, \bar{\mathbf{F}}^\tau, 0), \\ \mathbf{B}_1^{\bar{\tau}} &= \text{Diag}(\mathbf{U}^{\bar{\tau}}, \mathbf{U}^{\bar{\tau}}, \mathbf{U}^{\bar{\tau}}, \mathbf{U}^{\bar{\tau}}), \mathbf{B}_2^{\bar{\tau}} = \text{Diag}(\mathbf{V}^{\bar{\tau}}, \mathbf{F}^{\bar{\tau}}, \bar{\mathbf{F}}^{\bar{\tau}}, \mathbf{E}^{\bar{\tau}}), \\ \mathbf{C}^{\bar{\tau}} &= \text{Diag}(\mathbf{X}^{\bar{\tau}}, \bar{\mathbf{X}}^{\bar{\tau}}, \bar{\mathbf{X}}^{\bar{\tau}}, 0), \bar{\mathbf{\Lambda}}^\tau = \text{Diag}(\mathbf{G}^\tau, \bar{\mathbf{G}}^\tau, \mathbf{H}^\tau), \\ \bar{\mathbf{\Lambda}}^{\bar{\tau}} &= \text{Diag}(\mathbf{Q}^{\bar{\tau}}, \mathbf{G}^{\bar{\tau}}, \bar{\mathbf{G}}^{\bar{\tau}}, \mathbf{H}^{\bar{\tau}}). \end{aligned} \quad (60)$$

Let

$$\hat{\mathbf{U}}^{\tau(t+1,t)} = \text{Diag}(\mathbf{U}^{\tau(t+1)} - \mathbf{U}^{\tau(t)}, 0). \quad (61)$$

Combined with the optimality conditions of \mathbf{U} -subproblem, we have the below optimality conditions of \mathbf{B}_1 -subproblem

$$\begin{aligned} 0 &= \nabla f_1(\bar{\mathbf{B}}_1^{\tau(t+1)}) + \sigma \bar{\mathbf{A}}_1^\top (\bar{\mathbf{A}}_1 \bar{\mathbf{B}}_1^{\tau(t+1)} - \bar{\mathbf{B}}_2^{\tau(t+1)} \\ & \quad - \bar{\mathbf{C}}^\tau + \frac{1}{\sigma} \bar{\mathbf{\Lambda}}^{\tau(t)}), \\ 0 &= \sigma \mathbf{A}_1^\top (\mathbf{A}_1 \mathbf{B}_1^{\bar{\tau}(t+1)} + \mathbf{A}_2 \mathbf{B}_2^{\bar{\tau}(t+1)} - \mathbf{C}^{\bar{\tau}} \\ & \quad + \frac{1}{\sigma} \bar{\mathbf{\Lambda}}^{\bar{\tau}(t)}) + \gamma \hat{\mathbf{U}}^{\bar{\tau}(t+1,t)}, \end{aligned} \quad (62)$$

then, we get

$$\begin{aligned} \bar{\mathbf{A}}_1^\top \bar{\mathbf{\Lambda}}^{\tau(t+1)} &= -\nabla f_1(\bar{\mathbf{B}}_1^{\tau(t+1)}), \\ \mathbf{A}_1^\top \bar{\mathbf{\Lambda}}^{\bar{\tau}(t+1)} &= -\gamma \hat{\mathbf{U}}^{\bar{\tau}(t+1,t)}, \end{aligned} \quad (63)$$

which implies that

$$\begin{aligned}
& \|\mathbf{\Lambda}^{(t+1)} - \mathbf{\Lambda}^{(t)}\|_F^2 \\
&= \|\bar{\mathbf{\Lambda}}^{\tau(t+1)} - \bar{\mathbf{\Lambda}}^{\tau(t)}\|_F^2 + \|\mathbf{\Lambda}^{\bar{\tau}(t+1)} - \mathbf{\Lambda}^{\bar{\tau}(t)}\|_F^2 \\
&\leq \frac{1}{\lambda_+(\bar{\mathbf{A}}_1^\top \bar{\mathbf{A}}_1)} \|\bar{\mathbf{A}}_1^\top \bar{\mathbf{\Lambda}}^{\tau(t+1)} - \bar{\mathbf{A}}_1^\top \bar{\mathbf{\Lambda}}^{\tau(t)}\|_F^2 \\
&\quad + \frac{1}{\lambda_+(\mathbf{A}_1^\top \mathbf{A}_1)} \|\mathbf{A}_1^\top \mathbf{\Lambda}^{\bar{\tau}(t+1)} - \mathbf{A}_1^\top \mathbf{\Lambda}^{\bar{\tau}(t)}\|_F^2 \\
&= \|\bar{\mathbf{A}}_1^\top \bar{\mathbf{\Lambda}}^{\tau(t+1)} - \bar{\mathbf{A}}_1^\top \bar{\mathbf{\Lambda}}^{\tau(t)}\|_F^2 + \|\mathbf{A}_1^\top \mathbf{\Lambda}^{\bar{\tau}(t+1)} - \mathbf{A}_1^\top \mathbf{\Lambda}^{\bar{\tau}(t)}\|_F^2 \\
&\leq \|\nabla f_1(\bar{\mathbf{B}}_1^{\tau(t+1)}) - \nabla f_1(\bar{\mathbf{B}}_1^{\tau(t)})\|_F^2 + 2\gamma^2 \|\hat{\mathbf{U}}^{\bar{\tau}(t+1,t)}\|_F^2 \\
&\quad + 2\gamma^2 \|\hat{\mathbf{U}}^{\bar{\tau}(t,t-1)}\|_F^2 \\
&\leq l_u^2 \|\mathbf{U}^{\tau(t+1)} - \mathbf{U}^{\tau(t)}\|_F^2 + 2\gamma^2 \|\mathbf{U}^{\bar{\tau}(t+1)} - \mathbf{U}^{\bar{\tau}(t)}\|_F^2 \\
&\quad + 2\gamma^2 \|\mathbf{U}^{\bar{\tau}(t)} - \mathbf{U}^{\bar{\tau}(t-1)}\|_F^2,
\end{aligned} \tag{64}$$

where the first “ \leq ” holds via Assumption 3 and [41, Lemma 3], the second “=” holds via $\lambda_+(\bar{\mathbf{A}}_1^\top \bar{\mathbf{A}}_1) = \lambda_+(\mathbf{A}_1^\top \mathbf{A}_1) = 1$, the second “ \leq ” holds via $(\sum_{i=1}^n a_i)^2 \leq n(\sum_{i=1}^n a_i^2)$, and the third “ \leq ” holds via Assumption 1.

Then, we get

$$\begin{aligned}
& \hat{\mathcal{L}}_\sigma(\bar{\mathbf{Y}}^{(t+1)}, \mathbf{U}^{\bar{\tau}(t)}) - \hat{\mathcal{L}}_\sigma(\mathbf{B}_2^{(t+1)}, \mathbf{B}_1^{(t+1)}; \mathbf{\Lambda}^{(t)}, \mathbf{U}^{\bar{\tau}(t-1)}) \\
&= \langle \mathbf{A}_1 \mathbf{B}_1^{(t+1)} + \mathbf{A}_2 \mathbf{B}_2^{(t+1)} - \mathbf{C}, \mathbf{\Lambda}^{(t+1)} - \mathbf{\Lambda}^{(t)} \rangle \\
&\quad + \frac{2\gamma^2}{\sigma} (\|\mathbf{U}^{\bar{\tau}(t+1)} - \mathbf{U}^{\bar{\tau}(t)}\|_F^2 - \|\mathbf{U}^{\bar{\tau}(t+1)} - \mathbf{U}^{\bar{\tau}(t-1)}\|_F^2) \\
&= \frac{1}{\sigma} \|\mathbf{\Lambda}^{(t+1)} - \mathbf{\Lambda}^{(t)}\|_F^2 + \frac{2\gamma^2}{\sigma} (\|\mathbf{U}^{\bar{\tau}(t+1)} - \mathbf{U}^{\bar{\tau}(t)}\|_F^2 \\
&\quad - \|\mathbf{U}^{\bar{\tau}(t+1)} - \mathbf{U}^{\bar{\tau}(t-1)}\|_F^2) \\
&\leq \frac{l_u^2}{\sigma} \|\mathbf{U}^{\tau(t+1)} - \mathbf{U}^{\tau(t)}\|_F^2 + \frac{4\gamma^2}{\sigma} \|\mathbf{U}^{\bar{\tau}(t+1)} - \mathbf{U}^{\bar{\tau}(t)}\|_F^2 \\
&\quad + \frac{2\gamma^2}{\sigma} \|\mathbf{U}^{\bar{\tau}(t)} - \mathbf{U}^{\bar{\tau}(t-1)}\|_F^2 - \frac{2\gamma^2}{\sigma} \|\mathbf{U}^{\bar{\tau}(t+1)} - \mathbf{U}^{\bar{\tau}(t-1)}\|_F^2.
\end{aligned} \tag{65}$$

Due to the strong convexity of \mathbf{U}^τ -subproblem and $\mathbf{U}^{\bar{\tau}}$ -subproblem, and

$$\begin{aligned}
& f_2(\mathbf{B}_2^{(t+1)}) + \frac{\sigma}{2} \|\mathbf{A}_1 \mathbf{B}_1^{(t)} + \mathbf{A}_2 \mathbf{B}_2^{(t+1)} - \mathbf{C} + \frac{1}{\sigma} \mathbf{\Lambda}^{(t)}\|_F^2 \\
&\leq f_2(\mathbf{B}_2^{(t)}) + \frac{\sigma}{2} \|\mathbf{A}_1 \mathbf{B}_1^{(t)} + \mathbf{A}_2 \mathbf{B}_2^{(t)} - \mathbf{C} + \frac{1}{\sigma} \mathbf{\Lambda}^{(t)}\|_F^2,
\end{aligned} \tag{66}$$

we derive that

$$\begin{aligned}
& \hat{\mathcal{L}}_\sigma(\mathbf{B}_2^{(t+1)}, \mathbf{B}_1^{(t+1)}; \mathbf{\Lambda}^{(t)}, \mathbf{U}^{\bar{\tau}(t-1)}) \\
&\quad - \hat{\mathcal{L}}_\sigma(\mathbf{B}_2^{(t+1)}, \mathbf{B}_1^{(t)}; \mathbf{\Lambda}^{(t)}, \mathbf{U}^{\bar{\tau}(t-1)}) \\
&\leq f_1(\bar{\mathbf{B}}_1^{\tau(t+1)}) - f_1(\bar{\mathbf{B}}_1^{\tau(t)}) + \frac{\sigma}{2} \|\mathbf{A}_1 \mathbf{B}_1^{(t+1)} + \mathbf{A}_2 \mathbf{B}_2^{(t+1)} \\
&\quad - \mathbf{C}\|_F^2 - \frac{\sigma}{2} \|\mathbf{A}_1 \mathbf{B}_1^{(t)} + \mathbf{A}_2 \mathbf{B}_2^{(t+1)} - \mathbf{C}\|_F^2 \\
&\quad + \frac{2\gamma^2}{\sigma} (\|\mathbf{U}^{\bar{\tau}(t+1)} - \mathbf{U}^{\bar{\tau}(t-1)}\|_F^2 - \|\mathbf{U}^{\bar{\tau}(t)} - \mathbf{U}^{\bar{\tau}(t-1)}\|_F^2) \\
&\leq -\frac{3\sigma}{2} \|\mathbf{U}^{\tau(t+1)} - \mathbf{U}^{\tau(t)}\|_F^2 - 2\sigma \|\mathbf{U}^{\bar{\tau}(t+1)} - \mathbf{U}^{\bar{\tau}(t)}\|_F^2 \\
&\quad + \frac{2\gamma^2}{\sigma} (\|\mathbf{U}^{\bar{\tau}(t+1)} - \mathbf{U}^{\bar{\tau}(t-1)}\|_F^2 - \|\mathbf{U}^{\bar{\tau}(t)} - \mathbf{U}^{\bar{\tau}(t-1)}\|_F^2),
\end{aligned} \tag{67}$$

and

$$\hat{\mathcal{L}}_\sigma(\mathbf{B}_2^{(t+1)}, \mathbf{B}_1^{(t)}; \mathbf{\Lambda}^{(t)}, \mathbf{U}^{\bar{\tau}(t-1)}) - \hat{\mathcal{L}}_\sigma(\bar{\mathbf{Y}}^{(t)}, \mathbf{U}^{\bar{\tau}(t-1)}) \leq 0. \tag{68}$$

Summing both sides of (65), (67), and (68), we can obtain

$$\begin{aligned}
& \hat{\mathcal{L}}_\sigma(\bar{\mathbf{Y}}^{(t+1)}, \mathbf{U}^{\bar{\tau}(t)}) - \hat{\mathcal{L}}_\sigma(\bar{\mathbf{Y}}^{(t)}, \mathbf{U}^{\bar{\tau}(t-1)}) \\
&\leq -\left(\frac{3\sigma}{2} - \frac{l_u^2}{\sigma}\right) \|\mathbf{U}^{\tau(t+1)} - \mathbf{U}^{\tau(t)}\|_F^2 \\
&\quad - \left(2\sigma - \frac{4\gamma^2}{\sigma}\right) \|\mathbf{U}^{\bar{\tau}(t+1)} - \mathbf{U}^{\bar{\tau}(t)}\|_F^2 \\
&\leq -\bar{w} \|\mathbf{U}^{\tau(t+1)} - \mathbf{U}^{\tau(t)}\|_F^2,
\end{aligned} \tag{69}$$

where $\bar{w} = \min\{\frac{3\sigma}{2} - \frac{l_u^2}{\sigma}, 2\sigma - \frac{4\gamma^2}{\sigma}\}$. It guarantees the descent property of $\hat{\mathcal{L}}_\sigma$ if Assumptions 1 and Assumptions 2 hold.

2) According to (36), the below inclusion relationships hold

$$\begin{aligned}
& 0 \in \partial f_2(\mathbf{B}_2^{(t+1)}) \\
& \quad + \sigma \mathbf{A}_2^\top (\mathbf{A}_1 \mathbf{B}_1^{(t)} + \mathbf{A}_2 \mathbf{B}_2^{(t+1)} - \mathbf{C} + \frac{1}{\sigma} \mathbf{\Lambda}^{(t)}).
\end{aligned} \tag{70}$$

Then, the subdifferential of $\partial \hat{\mathcal{L}}_\sigma(\bar{\mathbf{Y}}^{(t)}, \mathbf{U}^{\bar{\tau}(t-1)})$ with respect to $\mathbf{B}_2^{(t)}$, $\bar{\mathbf{B}}_1^{\tau(t)}$, $\mathbf{B}_1^{\bar{\tau}(t)}$, and $\mathbf{\Lambda}^{(t)}$ can be represented as

$$\begin{cases} \partial_{\mathbf{B}_2} \hat{\mathcal{L}}_\sigma = \partial f_2(\mathbf{B}_2^{(t)}) + \mathbf{A}_2^\top (\mathbf{\Lambda}^{(t)} - \mathbf{\Lambda}^{(t-1)}) + \mathbf{A}_2^\top \mathbf{\Lambda}^{(t)}, \\ \partial_{\bar{\mathbf{B}}_1} \hat{\mathcal{L}}_\sigma = \nabla f_1(\bar{\mathbf{B}}_1^{\tau(t)}) + \bar{\mathbf{A}}_1^\top (\bar{\mathbf{\Lambda}}^{\tau(t)} - \bar{\mathbf{\Lambda}}^{\tau(t-1)}) + \bar{\mathbf{A}}_1^\top \bar{\mathbf{\Lambda}}^{\tau(t)}, \\ \partial_{\mathbf{B}_1} \hat{\mathcal{L}}_\sigma = \mathbf{A}_1^\top (\mathbf{\Lambda}^{\bar{\tau}(t)} - \mathbf{\Lambda}^{\bar{\tau}(t-1)}) + \mathbf{A}_1^\top \mathbf{\Lambda}^{\bar{\tau}(t)} + \frac{4\gamma^2}{\sigma} \hat{\mathbf{U}}^{\bar{\tau}(t,t-1)}, \\ \partial_{\mathbf{\Lambda}} \hat{\mathcal{L}}_\sigma = \frac{1}{\sigma} (\mathbf{\Lambda}^{(t)} - \mathbf{\Lambda}^{(t-1)}), \end{cases} \tag{71}$$

By combining (10), (62), (70) with (71), we have

$$\begin{cases} \partial_{\mathbf{B}_2} \hat{\mathcal{L}}_\sigma \ni \sigma \mathbf{A}_2^\top \mathbf{A}_1 (\mathbf{B}_1^{(t)} - \mathbf{B}_1^{(t-1)}) + \mathbf{A}_2^\top (\mathbf{\Lambda}^{(t)} - \mathbf{\Lambda}^{(t-1)}), \\ \partial_{\bar{\mathbf{B}}_1} \hat{\mathcal{L}}_\sigma = \bar{\mathbf{A}}_1^\top (\bar{\mathbf{\Lambda}}^{\tau(t)} - \bar{\mathbf{\Lambda}}^{\tau(t-1)}), \\ \partial_{\mathbf{B}_1} \hat{\mathcal{L}}_\sigma = (\frac{4\gamma^2}{\sigma} - \gamma) \hat{\mathbf{U}}^{\bar{\tau}(t,t-1)} + \mathbf{A}_1^\top (\mathbf{\Lambda}^{\bar{\tau}(t)} - \mathbf{\Lambda}^{\bar{\tau}(t-1)}). \end{cases} \tag{72}$$

It further follows from (63) that

$$\begin{aligned}
& \|\mathbf{\Lambda}^{(t)} - \mathbf{\Lambda}^{(t-1)}\|_F \\
&\leq \|\bar{\mathbf{A}}_1^\top \bar{\mathbf{\Lambda}}^{\tau(t)} - \bar{\mathbf{A}}_1^\top \bar{\mathbf{\Lambda}}^{\tau(t-1)}\|_F + \|\mathbf{A}_1^\top \mathbf{\Lambda}^{\bar{\tau}(t)} - \mathbf{A}_1^\top \mathbf{\Lambda}^{\bar{\tau}(t-1)}\|_F \\
&\leq \|\nabla f_1(\bar{\mathbf{B}}_1^{\tau(t)}) - \nabla f_1(\bar{\mathbf{B}}_1^{\tau(t-1)})\|_F + \gamma \|\hat{\mathbf{U}}^{\bar{\tau}(t,t-1)}\|_F \\
&\quad + \gamma \|\hat{\mathbf{U}}^{\bar{\tau}(t-1,t-2)}\|_F \\
&\leq l_u \|\mathbf{U}^{\tau(t)} - \mathbf{U}^{\tau(t-1)}\|_F + \gamma \|\mathbf{U}^{\bar{\tau}(t)} - \mathbf{U}^{\bar{\tau}(t-1)}\|_F \\
&\quad + \gamma \|\mathbf{U}^{\bar{\tau}(t-1)} - \mathbf{U}^{\bar{\tau}(t-2)}\|_F.
\end{aligned} \tag{73}$$

Thus,

$$\begin{aligned}
& d(0, \partial \hat{\mathcal{L}}_\sigma(\tilde{\mathbf{Y}}^{(t)}, \mathbf{U}^{\bar{\tau}(t-1)})) \\
& \leq \|\overrightarrow{\partial_{\mathbf{B}_2} \hat{\mathcal{L}}_\sigma}, \overrightarrow{\partial_{\mathbf{B}_1} \hat{\mathcal{L}}_\sigma}, \overrightarrow{\partial_{\Lambda} \hat{\mathcal{L}}_\sigma}\|_F \\
& \leq \left(\sigma + \frac{4\gamma^2}{\sigma} + \gamma\right) \|\mathbf{U}^{\bar{\tau}(t)} - \mathbf{U}^{\bar{\tau}(t-1)}\|_F \\
& \quad + \sqrt{2\sigma + \lambda_{\max}(\mathbf{D}^\top \mathbf{D})} \|\mathbf{U}^{(t)} - \mathbf{U}^{(t-1)}\|_F \\
& \quad + \left(1 + \frac{1}{\sigma} + \sqrt{\lambda_{\max}(\mathbf{A}_1^\top \mathbf{A}_1)}\right) \|\Lambda^{(t)} - \Lambda^{(t-1)}\|_F \\
& \leq \left(\sigma + \frac{4\gamma^2 + \gamma}{\sigma} + 2\gamma + \sqrt{\lambda_{\max}(\mathbf{D}^\top \mathbf{D})\gamma}\right) \|\mathbf{U}^{\bar{\tau}(t)} \\
& \quad - \mathbf{U}^{\bar{\tau}(t-1)}\|_F + \sqrt{2\sigma + \lambda_{\max}(\mathbf{D}^\top \mathbf{D})} \|\mathbf{U}^{(t)} - \mathbf{U}^{(t-1)}\|_F \\
& \quad + \left(l_u + \frac{l_u}{\sigma} + \sqrt{\lambda_{\max}(\mathbf{D}^\top \mathbf{D})l_u}\right) \|\mathbf{U}^{\tau(t)} - \mathbf{U}^{\tau(t-1)}\|_F \\
& \quad + \left(\gamma + \frac{\gamma}{\sigma} + \sqrt{\lambda_{\max}(\mathbf{D}^\top \mathbf{D})\gamma}\right) \|\mathbf{U}^{\bar{\tau}(t-1)} - \mathbf{U}^{\bar{\tau}(t-2)}\|_F \\
& \leq \tilde{w} \|\mathbf{U}^{(t)} - \mathbf{U}^{(t-1)}\|_F + \|\mathbf{U}^{(t-1)} - \mathbf{U}^{(t-2)}\|_F, \tag{74}
\end{aligned}$$

where the third “ \leq ” holds via (73), $\lambda_{\max}(\mathbf{A}_1^\top \mathbf{A}_1) = \lambda_{\max}(\mathbf{D}^\top \mathbf{D}) \geq 1$, and $\sum_{i=1}^n a_i \leq \sqrt{n} \sqrt{\sum_{i=1}^n (a_i)^2}$ when $a_i > 0$. ■

THE PROOF OF LEMMA 2

Proof: 1) Based on (63) and (64), we have

$$\begin{aligned}
\|\Lambda^{(t)}\|_F^2 &= \|\bar{\Lambda}^{\tau(t)}\|_F^2 + \|\Lambda^{\bar{\tau}(t)}\|_F^2 \\
&\leq \|\nabla L_\tau(\mathbf{U}^{\tau(t)})\|_F^2 + \gamma^2 \|\mathbf{U}^{\bar{\tau}(t)} - \mathbf{U}^{\bar{\tau}(t-1)}\|_F^2 \tag{75} \\
&\leq \bar{\pi}^2 + \gamma^2 \|\mathbf{U}^{\bar{\tau}(t)} - \mathbf{U}^{\bar{\tau}(t-1)}\|_F^2,
\end{aligned}$$

where $\|\nabla L_\tau(\cdot)\| \leq \bar{\pi}$ for $\bar{\pi} > 0$ because of the Lipschitz continuity of $\nabla L_\tau(\cdot)$ on its domain.

A combination of (75) and Lemma 1 makes

$$\begin{aligned}
& \hat{\mathcal{L}}_\sigma(\tilde{\mathbf{Y}}^{(1)}, \mathbf{U}^{\bar{\tau}(0)}) \geq \dots \geq \hat{\mathcal{L}}_\sigma(\tilde{\mathbf{Y}}^{(t)}, \mathbf{U}^{\bar{\tau}(t-1)}) \\
&= f(\mathbf{Y}_1^{(t)}, \mathbf{U}^{(t)}) + \frac{\sigma}{2} \|\mathbf{A}_1 \mathbf{B}_1^{(t)} + \mathbf{A}_2 \mathbf{B}_2^{(t)} - \mathbf{C} + \frac{1}{\sigma} \Lambda^{(t)}\|_F^2 \\
&\quad - \frac{1}{2\sigma} \|\Lambda^{(t)}\|_F^2 + \frac{2\gamma^2}{\sigma} \|\mathbf{U}^{\bar{\tau}(t)} - \mathbf{U}^{\bar{\tau}(t-1)}\|_F^2 \\
&\geq f(\mathbf{Y}_1^{(t)}, \mathbf{U}^{(t)}) + \frac{\sigma}{2} \|\mathbf{A}_1 \mathbf{B}_1^{(t)} + \mathbf{A}_2 \mathbf{B}_2^{(t)} - \mathbf{C} + \frac{1}{\sigma} \Lambda^{(t)}\|_F^2 \\
&\quad - \frac{\bar{\pi}^2}{2\sigma} + \frac{3\gamma^2}{2\sigma} \|\mathbf{U}^{\bar{\tau}(t)} - \mathbf{U}^{\bar{\tau}(t-1)}\|_F^2. \tag{76}
\end{aligned}$$

Then, $\hat{\mathcal{L}}_\sigma(\tilde{\mathbf{Y}}^{(t)}, \mathbf{U}^{\bar{\tau}(t-1)})$ is bounded from below and lower semi-continuous since $\hat{\mathcal{L}}_\sigma(\tilde{\mathbf{Y}}^{(1)}, \mathbf{U}^{\bar{\tau}(0)}) < +\infty$ and Assumption 4 holds. And, it is obvious that the generated sequence $\{\mathbf{Y}^{(t)}\}_{t=1}^\infty$ is bounded.

2) In accordance with Lemma 2 1) and the Bolzano-Weierstrass theorem, there exists at least one cluster point $\tilde{\mathbf{Y}} = (\tilde{\mathbf{Y}}_1, \tilde{\mathbf{U}}; \tilde{\mathbf{Y}}_2)$ and a subsequence $\{\mathbf{Y}^{(t_j)} = (\mathbf{Y}_1^{(t_j)}, \mathbf{U}^{(t_j)}; \mathbf{Y}_2^{(t_j)})\} \subseteq \{\mathbf{Y}^{(t)}\}$ such that

$$\lim_{j \rightarrow +\infty} \mathbf{Y}^{(t_j)} = \tilde{\mathbf{Y}}, \tag{77}$$

where $\tilde{\mathbf{Y}}_1 = (\tilde{\mathbf{V}}^{\bar{\tau}}, \tilde{\mathbf{F}}, \tilde{\mathbf{F}}, \tilde{\mathbf{E}})$ and $\tilde{\mathbf{Y}}_2 = (\tilde{\mathbf{Q}}^{\bar{\tau}}, \tilde{\mathbf{G}}, \tilde{\mathbf{G}}, \tilde{\mathbf{H}})$.

Naturally, $\tilde{\mathbf{Y}} = (\tilde{\mathbf{B}}_2, \tilde{\mathbf{B}}_1; \tilde{\Lambda})$ is the convergence point of a subsequence $\{\tilde{\mathbf{Y}}^{(t_j)} = (\mathbf{B}_2^{(t_j)}, \mathbf{B}_1^{(t_j)}, \Lambda^{(t_j)})\} \subseteq \{\tilde{\mathbf{Y}}^{(t)}\}$, i.e.,

$$\lim_{j \rightarrow +\infty} \tilde{\mathbf{Y}}^{(t_j)} = \tilde{\mathbf{Y}}, \tag{78}$$

where $\tilde{\mathbf{B}}_1$ consists of $\tilde{\mathbf{B}}_1^{\bar{\tau}}$ and $\tilde{\mathbf{B}}_1^{\bar{\tau}}$.

From the properness and the lower semi-continuity of $\hat{\mathcal{L}}_\sigma(\cdot, \cdot)$, we can get

$$\liminf_{j \rightarrow +\infty} \hat{\mathcal{L}}_\sigma(\tilde{\mathbf{Y}}^{(t_j)}, \mathbf{U}^{\bar{\tau}(t_j-1)}) \geq \mathcal{L}_\sigma(\tilde{\mathbf{Y}}) > -\infty. \tag{79}$$

Using Lemma 1, we have

$$\begin{aligned}
& \sum_{t=1}^{t_j-1} \|\mathbf{U}^{(t+1)} - \mathbf{U}^{(t)}\|_F^2 \\
& \leq \frac{1}{\tilde{w}} \sum_{t=1}^{t_j-1} (\hat{\mathcal{L}}_\sigma(\tilde{\mathbf{Y}}^{(t)}, \mathbf{U}^{\bar{\tau}(t-1)}) - \hat{\mathcal{L}}_\sigma(\tilde{\mathbf{Y}}^{(t+1)}, \mathbf{U}^{\bar{\tau}(t)})) \tag{80} \\
& \leq \frac{1}{\tilde{w}} (\hat{\mathcal{L}}_\sigma(\tilde{\mathbf{Y}}^{(1)}, \mathbf{U}^{\bar{\tau}(0)}) - \hat{\mathcal{L}}_\sigma(\tilde{\mathbf{Y}}^{(t_j)}, \mathbf{U}^{\bar{\tau}(t_j-1)})),
\end{aligned}$$

which indicates that

$$\sum_{t=1}^{+\infty} \|\mathbf{U}^{(t+1)} - \mathbf{U}^{(t)}\|_F^2 < +\infty \text{ as } j \rightarrow +\infty. \tag{81}$$

Subsequently, it holds from (64) and Assumption 2 that

$$\begin{aligned}
& \sum_{t=1}^{+\infty} \|\mathbf{Y}_2^{(t+1)} - \mathbf{Y}_2^{(t)}\|_F^2 = \sum_{t=1}^{+\infty} \|\Lambda^{(t+1)} - \Lambda^{(t)}\|_F^2 \\
& \leq \max\{l_u^2, 2\gamma^2\} \sum_{t=1}^{+\infty} (\|\mathbf{U}^{(t+1)} - \mathbf{U}^{(t)}\|_F^2 + \|\mathbf{U}^{(t)} - \mathbf{U}^{(t-1)}\|_F^2) \\
& < +\infty. \tag{82}
\end{aligned}$$

Further, we obtain with (59) that

$$\begin{aligned}
& \|\bar{\mathbf{B}}_2^{\tau(t+1)} - \bar{\mathbf{B}}_2^{\tau(t)}\|_F \\
& \leq \frac{1}{\sigma} (\|\bar{\Lambda}^{\tau(t+1)} - \bar{\Lambda}^{\tau(t)}\|_F + \|\bar{\Lambda}^{\tau(t)} - \bar{\Lambda}^{\tau(t-1)}\|_F) \tag{83} \\
& \quad + \sqrt{\lambda_{\max}(\mathbf{D}^\top \mathbf{D})} \|\bar{\mathbf{B}}_1^{\tau(t+1)} - \bar{\mathbf{B}}_1^{\tau(t)}\|_F,
\end{aligned}$$

and

$$\begin{aligned}
& \|\mathbf{B}_2^{\bar{\tau}(t+1)} - \mathbf{B}_2^{\bar{\tau}(t)}\|_F = \|\mathbf{A}_2(\mathbf{B}_2^{\bar{\tau}(t+1)} - \mathbf{B}_2^{\bar{\tau}(t)})\|_F \\
& \leq \frac{1}{\sigma} (\|\Lambda^{\bar{\tau}(t+1)} - \Lambda^{\bar{\tau}(t)}\|_F + \|\Lambda^{\bar{\tau}(t)} - \Lambda^{\bar{\tau}(t-1)}\|_F) \tag{84} \\
& \quad + \sqrt{\lambda_{\max}(\mathbf{D}^\top \mathbf{D})} \|\mathbf{B}_1^{\bar{\tau}(t+1)} - \mathbf{B}_1^{\bar{\tau}(t)}\|_F.
\end{aligned}$$

We can conclude

$$\begin{aligned}
& \sum_{t=1}^{+\infty} \|\mathbf{Y}_1^{(t+1)} - \mathbf{Y}_1^{(t)}\|_F^2 = \sum_{t=1}^{+\infty} \|\mathbf{B}_2^{(t+1)} - \mathbf{B}_2^{(t)}\|_F^2 \\
&= \sum_{t=1}^{+\infty} (\|\bar{\mathbf{B}}_2^{\tau(t+1)} - \bar{\mathbf{B}}_2^{\tau(t)}\|_F^2 + \|\mathbf{B}_2^{\bar{\tau}(t+1)} - \mathbf{B}_2^{\bar{\tau}(t)}\|_F^2) \tag{85} \\
&\leq \sum_{t=1}^{+\infty} \left(\frac{3}{\sigma} \|\Lambda^{(t+1)} - \Lambda^{(t)}\|_F^2 + \frac{3}{\sigma} \|\Lambda^{(t)} - \Lambda^{(t-1)}\|_F^2\right. \\
&\quad \left.+ 12\lambda_{\max}(\mathbf{D}^\top \mathbf{D}) \|\mathbf{U}^{(t+1)} - \mathbf{U}^{(t)}\|_F^2\right) \\
&< +\infty.
\end{aligned}$$

Therefore, it follows from (78) that

$$\lim_{t \rightarrow +\infty} (\mathbf{Y}^{(t+1)} - \mathbf{Y}^{(t)}) = 0, \quad (86)$$

which means that 2) holds. \blacksquare

THE PROOF OF THEOREM 2

Proof: 1) Lemma 2 2) and (78) suggest $\mathbf{Y}^{(t_j+1)} \rightarrow \tilde{\mathbf{Y}}$ as $j \rightarrow +\infty$. By virtue of the lower semi-continuity of $\mathcal{L}_\sigma(\cdot, \cdot)$, we get

$$\begin{aligned} & \liminf_{j \rightarrow +\infty} \mathcal{L}_\sigma(\mathbf{Y}^{(t_j+1)}) \geq \mathcal{L}_\sigma(\tilde{\mathbf{Y}}) \\ & = L_\tau(\tilde{\mathbf{U}}^\tau) + q(\tilde{\mathbf{V}}^{\bar{\tau}}) + p(\tilde{\mathbf{E}}) + r_1(\tilde{\mathbf{F}}) + r_2(\tilde{\mathbf{F}}) \\ & \quad + \frac{\sigma}{2} \|\mathbf{A}_1 \tilde{\mathbf{B}}_1 + \mathbf{A}_2 \tilde{\mathbf{B}}_2 - \mathbf{C} + \frac{1}{\sigma} \tilde{\Lambda}\|_F^2 - \frac{1}{2\sigma} \|\tilde{\Lambda}\|_F^2. \end{aligned} \quad (87)$$

Since $\mathbf{Y}_1^{(t_j+1)}$ is the minimizer of the \mathbf{Y}_1 -subproblem for (9), it holds

$$\begin{aligned} & \mathcal{L}_\sigma(\mathbf{Y}_1^{(t_j+1)}, \mathbf{U}^{(t_j)}; \mathbf{Y}_2^{(t_j)}) \\ & \leq \mathcal{L}_\sigma(\tilde{\mathbf{Y}}_1, \mathbf{U}^{(t_j)}; \mathbf{Y}_2^{(t_j)}) \\ & = L_\tau(\mathbf{U}^\tau(t_j)) + q(\tilde{\mathbf{V}}^{\bar{\tau}}) + p(\mathbf{E}^{(t_j)}) + r_1(\tilde{\mathbf{F}}) + r_2(\tilde{\mathbf{F}}) \\ & \quad + \frac{\sigma}{2} \|\mathbf{A}_1 \mathbf{B}_1^{(t_j)} + \mathbf{A}_2 \tilde{\mathbf{B}}_2 - \mathbf{C} + \frac{1}{\sigma} \Lambda^{(t_j)}\|_F^2 - \frac{1}{2\sigma} \|\Lambda^{(t_j)}\|_F^2. \end{aligned} \quad (88)$$

Based on the continuity of $L_\tau(\cdot)$, we find that

$$\limsup_{j \rightarrow +\infty} \mathcal{L}_\sigma(\mathbf{Y}_1^{(t_j+1)}, \mathbf{U}^{(t_j)}; \mathbf{Y}_2^{(t_j)}) \leq \mathcal{L}_\sigma(\tilde{\mathbf{Y}}). \quad (89)$$

Considering both (87) and (89), we can deduce

$$\begin{aligned} & \lim_{j \rightarrow +\infty} \mathcal{L}_\sigma(\mathbf{Y}_1^{(t_j+1)}, \mathbf{U}^{(t_j)}; \mathbf{Y}_2^{(t_j)}) \\ & = L_\tau(\tilde{\mathbf{U}}^\tau) + q(\tilde{\mathbf{V}}^{\bar{\tau}}) + p(\tilde{\mathbf{E}}) + r_1(\tilde{\mathbf{F}}) + r_2(\tilde{\mathbf{F}}) \\ & \quad + \frac{\sigma}{2} \|\tilde{\mathbf{B}}_1 + \mathbf{A}_2 \tilde{\mathbf{B}}_2 - \tilde{\mathbf{B}}_3 - \mathbf{C} + \frac{1}{\sigma} \tilde{\Lambda}\|_F^2 - \frac{1}{2\sigma} \|\tilde{\Lambda}\|_F^2. \end{aligned} \quad (90)$$

Further, it is easy to derive from the continuity of $q(\cdot)$ and $p(\cdot)$ that

$$\lim_{j \rightarrow +\infty} r_1(\mathbf{F}^{(t_j+1)}) + r_2(\tilde{\mathbf{F}}^{(t_j+1)}) = r_1(\tilde{\mathbf{F}}) + r_2(\tilde{\mathbf{F}}). \quad (91)$$

It follows from for (10) and (91) that

$$\begin{cases} 0 = \nabla L_\tau(\tilde{\mathbf{U}}^\tau) + \tilde{\mathbf{H}}^\tau + \tilde{\mathbf{G}}^\tau, \\ 0 = \tilde{\mathbf{Q}}^{\bar{\tau}} + \tilde{\mathbf{H}}^{\bar{\tau}} + \tilde{\mathbf{G}}^{\bar{\tau}}, \\ 0 \in \partial q(\tilde{\mathbf{V}}^{\bar{\tau}}) + \tilde{\mathbf{Q}}^{\bar{\tau}}, \\ 0 \in \partial p(\tilde{\mathbf{E}}) - \tilde{\mathbf{H}}, \\ 0 \in \partial(r_1(\tilde{\mathbf{F}}) + r_2(\tilde{\mathbf{F}})) - \tilde{\mathbf{G}}, \\ 0 = \tilde{\mathbf{U}}^{\bar{\tau}} + \tilde{\mathbf{V}}^{\bar{\tau}} - \mathbf{X}^{\bar{\tau}}, \\ 0 = \tilde{\mathbf{U}} - \tilde{\mathbf{X}} - \tilde{\mathbf{F}}, \\ 0 = \tilde{\mathbf{U}} - \tilde{\mathbf{E}}, \end{cases} \quad (92)$$

which implies that $\tilde{\mathbf{Y}}$ is a KKT point of (30) according to Theorem 1.

2) On account of the Assumption 4 and Lemma 1 1), we realize that $\{\hat{\mathcal{L}}_\sigma(\tilde{\mathbf{Y}}^{(t+1)}, \mathbf{U}^{\bar{\tau}(t)})\}_{t=1}^{+\infty}$ generated by the proposed Algorithm 1 is bounded from below and nonincreasing. So, there exists a constant \tilde{l} such that

$$\lim_{t \rightarrow +\infty} \hat{\mathcal{L}}_\sigma(\tilde{\mathbf{Y}}^{(t+1)}, \mathbf{U}^{\bar{\tau}(t)}) = \tilde{l}. \quad (93)$$

Let Γ denote the set of cluster points. Take $\forall \tilde{\mathbf{Y}} \in \Gamma$ and consider a converged subsequence satisfying (78), it follows from (87), (89), (93), and $\mathcal{L}_\sigma(\tilde{\mathbf{Y}}) = \mathcal{L}_\sigma(\mathbf{Y})$ that

$$\begin{aligned} \tilde{l} & = \liminf_{j \rightarrow +\infty} \hat{\mathcal{L}}_\sigma(\mathbf{B}_2^{(t_j+1)}, \mathbf{B}_1^{(t_j)}; \Lambda^{(t_j)}, \mathbf{U}^{\bar{\tau}(t_j)}) \geq \hat{\mathcal{L}}_\sigma(\tilde{\mathbf{Y}}, \tilde{\mathbf{U}}^{\bar{\tau}}), \\ \tilde{l} & = \limsup_{j \rightarrow +\infty} \hat{\mathcal{L}}_\sigma(\mathbf{B}_2^{(t_j+1)}, \mathbf{B}_1^{(t_j)}; \Lambda^{(t_j)}, \mathbf{U}^{\bar{\tau}(t_j)}) \leq \hat{\mathcal{L}}_\sigma(\tilde{\mathbf{Y}}, \tilde{\mathbf{U}}^{\bar{\tau}}), \end{aligned} \quad (94)$$

which shows that $\hat{\mathcal{L}}_\sigma(\tilde{\mathbf{Y}}, \tilde{\mathbf{U}}^{\bar{\tau}}) = \tilde{l}$. Because of the arbitrariness of $\tilde{\mathbf{Y}}$ in set Γ , we further infer that $\hat{\mathcal{L}}_\sigma(\cdot, \cdot)$ is constant on Γ . And, for given $l_1 > 0$, there exists $t_1 > 0$ such that $\hat{\mathcal{L}}_\sigma(\tilde{\mathbf{Y}}^{(t)}, \mathbf{U}^{\bar{\tau}(t-1)}) < \tilde{l} + l_1$ for $\forall t > t_1$. Simultaneously, $\hat{\mathcal{L}}_\sigma(\tilde{\mathbf{Y}}^{(t)}, \mathbf{U}^{\bar{\tau}(t-1)}) > \tilde{l}$ for $\forall t > 1$. In view of the definition of Γ , there exist $t_2 > 0$ and $\varepsilon > 0$ such that $\text{dist}(\tilde{\mathbf{Y}}^{(t)}, \Gamma) < \varepsilon$ for $\forall t > t_2$. Therefore, for KL function $\hat{\mathcal{L}}_\sigma(\cdot, \cdot)$, it follows [26] that for $\forall t > \bar{t}$, there exists $\wp \in \bar{\wp}$ such that

$$\wp'(\hat{\mathcal{L}}_\sigma(\tilde{\mathbf{Y}}^{(t)}, \mathbf{U}^{\bar{\tau}(t-1)}) - \tilde{l}) \text{dist}(0, \hat{\mathcal{L}}_\sigma(\tilde{\mathbf{Y}}^{(t)}, \mathbf{U}^{\bar{\tau}(t-1)})) \geq 1, \quad (95)$$

where $\bar{t} = \max\{t_1, t_2\}$.

Let $\Delta_{t,t+1} = \wp(\hat{\mathcal{L}}_\sigma(\tilde{\mathbf{Y}}^{(t)}, \mathbf{U}^{\bar{\tau}(t-1)}) - \tilde{l}) - \wp(\hat{\mathcal{L}}_\sigma(\tilde{\mathbf{Y}}^{(t+1)}, \mathbf{U}^{\bar{\tau}(t)}) - \tilde{l})$. Using Lemma 1 and the concavity of $\wp(\cdot)$, we get

$$\begin{aligned} & \tilde{w}(\|\mathbf{U}^{(t)} - \mathbf{U}^{(t-1)}\|_F + \|\mathbf{U}^{(t-1)} - \mathbf{U}^{(t-2)}\|_F) \Delta_{t,t+1} \\ & \geq \text{dist}(0, \partial \hat{\mathcal{L}}_\sigma(\tilde{\mathbf{Y}}^{(t)}, \mathbf{U}^{\bar{\tau}(t-1)})) \times \wp'(\hat{\mathcal{L}}_\sigma(\tilde{\mathbf{Y}}^{(t)}, \mathbf{U}^{\bar{\tau}(t-1)}) - \tilde{l}) \\ & \quad \times (\hat{\mathcal{L}}_\sigma(\tilde{\mathbf{Y}}^{(t)}, \mathbf{U}^{\bar{\tau}(t-1)}) - \hat{\mathcal{L}}_\sigma(\tilde{\mathbf{Y}}^{(t+1)}, \mathbf{U}^{\bar{\tau}(t)})) \\ & \geq \tilde{w} \|\mathbf{U}^{(t+1)} - \mathbf{U}^{(t)}\|_F^2, \end{aligned} \quad (96)$$

from which we can see

$$\begin{aligned} & 3 \|\mathbf{U}^{(t+1)} - \mathbf{U}^{(t)}\|_F \\ & \leq 3 \sqrt{\|\mathbf{U}^{(t+1)} - \mathbf{U}^{(t)}\|_F^2} \\ & \leq 2 \sqrt{\frac{9\tilde{w}}{4\tilde{w}} (\|\mathbf{U}^{(t)} - \mathbf{U}^{(t-1)}\|_F + \|\mathbf{U}^{(t-1)} - \mathbf{U}^{(t-2)}\|_F) \Delta_{t,t+1}} \\ & \leq \|\mathbf{U}^{(t)} - \mathbf{U}^{(t-1)}\|_F + \|\mathbf{U}^{(t-1)} - \mathbf{U}^{(t-2)}\|_F + \frac{9\tilde{w}}{4\tilde{w}} \Delta_{t,t+1}. \end{aligned} \quad (97)$$

Then,

$$\begin{aligned} & \sum_{t=\bar{t}}^{+\infty} \|\mathbf{U}^{(t+1)} - \mathbf{U}^{(t)}\|_F \\ & \leq 2 \|\mathbf{U}^{(\bar{t})} - \mathbf{U}^{(\bar{t}-1)}\|_F + \|\mathbf{U}^{(\bar{t}-1)} - \mathbf{U}^{(\bar{t}-2)}\|_F \\ & \quad + \frac{9\tilde{w}}{4\tilde{w}} \wp(\hat{\mathcal{L}}_\sigma(\tilde{\mathbf{Y}}^{(\bar{t})}, \mathbf{U}^{\bar{\tau}(\bar{t}-1)}) - \tilde{l}) \\ & < +\infty. \end{aligned} \quad (98)$$

Besides, it follows from (73), (83), and (84) that

$$\begin{aligned} & \sum_{t=\bar{t}}^{+\infty} \|\mathbf{Y}_2^{(t+1)} - \mathbf{Y}_2^{(t)}\|_F = \sum_{t=\bar{t}}^{+\infty} \|\Lambda^{(t+1)} - \Lambda^{(t)}\|_F \\ & \leq \sum_{t=\bar{t}+1}^{+\infty} (l_u \|\mathbf{U}^{\tau(t+1)} - \mathbf{U}^{\tau(t)}\|_F + \gamma \|\mathbf{U}^{\bar{\tau}(t+1)} - \mathbf{U}^{\bar{\tau}(t)}\|_F \\ & \quad + \gamma \|\mathbf{U}^{\bar{\tau}(t)} - \mathbf{U}^{\bar{\tau}(t-1)}\|_F) + \|\Lambda^{(\bar{t}+1)} - \Lambda^{(\bar{t})}\|_F \\ & < +\infty \end{aligned} \quad (99)$$

and

$$\begin{aligned}
& \sum_{t=\bar{t}}^{+\infty} \|\mathbf{r}_1^{(t+1)} - \mathbf{r}_1^{(t)}\|_F = \sum_{t=\bar{t}}^{+\infty} \|\mathbf{B}_2^{(t+1)} - \mathbf{B}_2^{(t)}\|_F \\
& \leq \sum_{t=\bar{t}}^{+\infty} (\|\bar{\mathbf{B}}_2^{\tau(t+1)} - \bar{\mathbf{B}}_2^{\tau(t)}\|_F + \|\mathbf{B}_2^{\bar{\tau}(t+1)} - \mathbf{B}_2^{\bar{\tau}(t)}\|_F) \\
& \leq \sqrt{2} \sum_{t=\bar{t}}^{+\infty} \left(\frac{1}{\sigma} \|\mathbf{\Lambda}^{(t+1)} - \mathbf{\Lambda}^{(t)}\|_F + \frac{1}{\sigma} \|\mathbf{\Lambda}^{(t)} - \mathbf{\Lambda}^{(t-1)}\|_F \right. \\
& \quad \left. + \|\mathbf{B}_1^{(t+1)} - \mathbf{B}_1^{(t)}\|_F \right) \\
& \leq \frac{2\sqrt{2}}{\sigma} \sum_{t=\bar{t}}^{+\infty} \|\mathbf{\Lambda}^{(t+1)} - \mathbf{\Lambda}^{(t)}\|_F + 4\sqrt{2} \sum_{t=\bar{t}}^{+\infty} \|\mathbf{U}^{(t+1)} - \mathbf{U}^{(t)}\|_F \\
& \quad + \frac{\sqrt{2}}{\sigma} \|\mathbf{\Lambda}^{(\bar{t})} - \mathbf{\Lambda}^{(\bar{t}-1)}\|_F \\
& < +\infty.
\end{aligned} \tag{100}$$

By combining (98)-(100) for the fixed \bar{t} , we deduce

$$\begin{aligned}
& \sum_{t=\bar{t}}^{+\infty} \|\mathbf{r}^{(t+1)} - \mathbf{r}^{(t)}\|_F \\
& = \sum_{t=\bar{t}}^{+\infty} (\|\mathbf{U}^{(t+1)} - \mathbf{U}^{(t)}\|_F^2 + \|\mathbf{r}_2^{(t+1)} - \mathbf{r}_2^{(t)}\|_F^2 \\
& \quad + \|\mathbf{r}_1^{(t+1)} - \mathbf{r}_1^{(t)}\|_F^2)^{\frac{1}{2}} \\
& \leq \sum_{t=\bar{t}}^{+\infty} (\|\mathbf{U}^{(t+1)} - \mathbf{U}^{(t)}\|_F + \|\mathbf{r}_2^{(t+1)} - \mathbf{r}_2^{(t)}\|_F \\
& \quad + \|\mathbf{r}_1^{(t+1)} - \mathbf{r}_1^{(t)}\|_F) \\
& < +\infty,
\end{aligned} \tag{101}$$

which implies that $\{\mathbf{r}^{(t)}\}_{t=\bar{t}}^{+\infty}$ is a Cauchy sequence and hence converges to a KKT point of (30). ■

REFERENCES

- [1] L. Zhou, G. Du, K. Lü, L. Wang, and J. Du, "A survey and an empirical evaluation of multi-view clustering approaches," *ACM Computing Surveys*, vol. 56, no. 7, pp. 1–38, 2024.
- [2] U. Fang, M. Li, J. Li, L. Gao, T. Jia, and Y. Zhang, "A comprehensive survey on multi-view clustering," *IEEE Transactions on Knowledge and Data Engineering*, vol. 35, no. 12, pp. 12 350–12 368, 2023.
- [3] Z. Yang and Y. Tan, "The methods for improving large-scale multi-view clustering efficiency: a survey," *Artificial Intelligence Review*, vol. 57, no. 6, p. 153, 2024.
- [4] Y. Song, P. Zhao, S. Wang, Q. Liao, and W. Yang, "Study of 3D finger vein biometrics on imaging device design and multi-view verification," *IEEE Transactions on Circuits and Systems for Video Technology*, vol. 34, no. 4, pp. 3043–3048, 2024.
- [5] Y. Wang, Y.-W. Zhan, Z.-D. Chen, X. Luo, and X.-S. Xu, "Multiple information embedded hashing for large-scale cross-modal retrieval," *IEEE Transactions on Circuits and Systems for Video Technology*, vol. 34, no. 6, pp. 5118–5131, 2024.
- [6] A. Huang, L. Li, L. Zhang, Y. Niu, T. Zhao, and C.-W. Lin, "Multi-view graph embedding learning for image co-segmentation and co-localization," *IEEE Transactions on Circuits and Systems for Video Technology*, vol. 34, no. 6, pp. 4942–4956, 2024.
- [7] J. Sun, X. Xiu, Z. Luo, and W. Liu, "Learning high-order multi-view representation by new tensor canonical correlation analysis," *IEEE Transactions on Circuits and Systems for Video Technology*, vol. 33, no. 10, pp. 5645–5654, 2023.
- [8] T. M. Tang and G. I. Allen, "Integrated principal components analysis," *Journal of Machine Learning Research*, vol. 22, no. 198, pp. 1–71, 2021.
- [9] H. Choi and S. Lee, "Convex clustering for binary data," *Advances in Data Analysis and Classification*, vol. 13, no. 4, pp. 991–1018, 2019.
- [10] S. Chu, H. Jiang, Z. Xue, and X. Deng, "Adaptive convex clustering of generalized linear models with application in purchase likelihood prediction," *Technometrics*, vol. 63, no. 2, pp. 171–183, 2021.
- [11] J. Zhao, X. Xie, X. Xu, and S. Sun, "Multi-view learning overview: Recent progress and new challenges," *Information Fusion*, vol. 38, pp. 43–54, 2017.
- [12] D. Ghosh and A. M. Chinnaiyan, "Mixture modelling of gene expression data from microarray experiments," *Bioinformatics*, vol. 18, no. 2, pp. 275–286, 2002.
- [13] L. Van der Maaten and G. Hinton, "Visualizing data using t-SNE," *Journal of Machine Learning Research*, vol. 9, no. 11, pp. 2579–2605, 2008.
- [14] J. Liu, C. Wang, J. Gao, and J. Han, "Multi-view clustering via joint nonnegative matrix factorization," in *Proceedings of the 2013 SIAM International Conference on Data Mining*. SIAM, 2013, pp. 252–260.
- [15] S.-G. Fang, D. Huang, C.-D. Wang, and Y. Tang, "Joint multi-view unsupervised feature selection and graph learning," *IEEE Transactions on Emerging Topics in Computational Intelligence*, vol. 8, no. 1, pp. 16–31, 2024.
- [16] Z. Zhao, T. Wang, H. Xin, R. Wang, and F. Nie, "Multi-view clustering via high-order bipartite graph fusion," *Information Fusion*, vol. 113, p. 102630, 2025.
- [17] M.-S. Yang and K. P. Sinaga, "Federated multi-view K-means clustering," *IEEE Transactions on Pattern Analysis and Machine Intelligence*, doi: 10.1109/TPAMI.2024.3520708.
- [18] S. Wang, Y. Chen, Z. Lin, Y. Cen, and Q. Cao, "Robustness meets low-rankness: Unified entropy and tensor learning for multi-view subspace clustering," *IEEE Transactions on Circuits and Systems for Video Technology*, vol. 33, no. 11, pp. 6302–6316, 2023.
- [19] D. Xie, Q. Gao, Y. Zhao, F. Yang, and W. Song, "Consistent graph learning for multi-view spectral clustering," *Pattern Recognition*, vol. 154, p. 110598, 2024.
- [20] X. Zhang, J. Zheng, D. Wang, G. Tang, Z. Zhou, and Z. Lin, "Structured sparsity optimization with non-convex surrogates of $\ell_{2,0}$ -norm: A unified algorithmic framework," *IEEE Transactions on Pattern Analysis and Machine Intelligence*, vol. 45, no. 5, pp. 6386–6402, 2023.
- [21] Y. Zhu, X. Xiu, W. Liu, and C. Yin, "Joint sparse subspace clustering via fast $\ell_{2,0}$ -norm constrained optimization," *Expert Systems with Applications*, vol. 265, p. 125845, 2025.
- [22] H. Zou and T. Hastie, "Regularization and variable selection via the elastic net," *Journal of the Royal Statistical Society Series B: Statistical Methodology*, vol. 67, no. 2, pp. 301–320, 2005.
- [23] M. Wang and G. I. Allen, "Integrative generalized convex clustering optimization and feature selection for mixed multi-view data," *Journal of Machine Learning Research*, vol. 22, no. 1, pp. 2498–2571, 2021.
- [24] H. Chen, L. Kong, and Y. Li, "Nonconvex clustering via ℓ_0 fusion penalized regression," *Pattern Recognition*, vol. 128, p. 108689, 2022.
- [25] Q. Tang and G. Li, "Sparse 10-norm least squares support vector machine with feature selection," *Information Sciences*, vol. 670, p. 120591, 2024.
- [26] H. Zhang, J. Gao, J. Qian, J. Yang, C. Xu, and B. Zhang, "Linear regression problem relaxations solved by nonconvex ADMM with convergence analysis," *IEEE Transactions on Circuits and Systems for Video Technology*, vol. 34, no. 2, pp. 828–838, 2024.
- [27] R. F. Barber and E. Y. Sidky, "Convergence for nonconvex ADMM, with applications to CT imaging," *Journal of Machine Learning Research*, vol. 25, no. 38, pp. 1–46, 2024.
- [28] A. Beck, *First-order methods in optimization*. SIAM, 2017.
- [29] K. Pelckmans, J. De Brabanter, J. A. Suykens, and B. De Moor, "Convex clustering shrinkage," in *PASCAL Workshop on Statistics and Optimization of Clustering Workshop*, 2005.
- [30] F. Lindsten, H. Ohlsson, and L. Ljung, "Clustering using sum-of-norms regularization: With application to particle filter output computation," in *2011 IEEE Statistical Signal Processing Workshop (SSP)*. IEEE, 2011, pp. 201–204.
- [31] D. Sun, K.-C. Toh, and Y. Yuan, "Convex clustering: Model, theoretical guarantee and efficient algorithm," *Journal of Machine Learning Research*, vol. 22, no. 1, pp. 427–458, 2021.
- [32] B. Wang, Y. Zhang, W. W. Sun, and Y. Fang, "Sparse convex clustering," *Journal of Computational and Graphical Statistics*, vol. 27, no. 2, pp. 393–403, 2018.
- [33] H. Chen, L. Kong, and Y. Li, "A novel convex clustering method for high-dimensional data using semiproximal ADMM," *Mathematical Problems in Engineering*, vol. 2020, pp. 1–12, 2020.

- [34] Q. Feng, C. P. Chen, and L. Liu, "A review of convex clustering from multiple perspectives: Models, optimizations, statistical properties, applications, and connections," *IEEE Transactions on Neural Networks and Learning Systems*, vol. 35, no. 10, pp. 13 122–13 142, 2024.
- [35] C. Liu, Q. Sun, and K. M. Tan, "Robust convex clustering: How does fusion penalty enhance robustness?" *arXiv preprint arXiv:1906.09581*, 2019.
- [36] T. Yao and G. I. Allen, "Clustered Gaussian graphical model via symmetric convex clustering," in *2019 IEEE Data Science Workshop (DSW)*. IEEE, 2019, pp. 76–82.
- [37] T. Wangchamhan, S. Chiewchanwattana, and K. Sunat, "Efficient algorithms based on the K-means and Chaotic League Championship algorithm for numeric, categorical, and mixed-type data clustering," *Expert Systems with Applications*, vol. 90, pp. 146–167, 2017.
- [38] Ö. Akay and G. Yüksel, "Clustering the mixed panel dataset using Gower's distance and k-prototypes algorithms," *Communications in Statistics-Simulation and Computation*, vol. 47, no. 10, pp. 3031–3041, 2018.
- [39] J. Fan and R. Li, "Variable selection via nonconcave penalized likelihood and its oracle properties," *Journal of the American Statistical Association*, vol. 96, no. 456, pp. 1348–1360, 2001.
- [40] C. Chen, B. He, Y. Ye, and X. Yuan, "The direct extension of ADMM for multi-block convex minimization problems is not necessarily convergent," *Mathematical Programming*, vol. 155, no. 1, pp. 57–79, 2016.
- [41] Y. Wang, W. Yin, and J. Zeng, "Global convergence of ADMM in nonconvex nonsmooth optimization," *Journal of Scientific Computing*, vol. 78, pp. 29–63, 2019.
- [42] Y. Yang, Q.-S. Jia, Z. Xu, X. Guan, and C. J. Spanos, "Proximal admm for nonconvex and nonsmooth optimization," *Automatica*, vol. 146, p. 110551, 2022.
- [43] H. Attouch, J. Bolte, and B. F. Svaiter, "Convergence of descent methods for semi-algebraic and tame problems: Proximal algorithms, forward-backward splitting, and regularized Gauss–Seidel methods," *Mathematical Programming*, vol. 137, no. 1, pp. 91–129, 2013.
- [44] L. Hubert and P. Arabie, "Comparing partitions," *Journal of Classification*, vol. 2, pp. 193–218, 1985.
- [45] E. B. Fowlkes and C. L. Mallows, "A method for comparing two hierarchical clusterings," *Journal of the American Statistical Association*, vol. 78, no. 383, pp. 553–569, 1983.
- [46] P. Zhang, X. Liu, J. Xiong, S. Zhou, W. Zhao, E. Zhu, and Z. Cai, "Consensus one-step multi-view subspace clustering," *IEEE Transactions on Knowledge and Data Engineering*, vol. 34, no. 10, pp. 4676–4689, 2022.
- [47] Z. Cao and X. Xie, "Structure learning with consensus label information for multi-view unsupervised feature selection," *Expert Systems with Applications*, vol. 238, p. 121893, 2024.
- [48] X. Chen, L. Guo, Z. Lu, and J. J. Ye, "An augmented Lagrangian method for non-Lipschitz nonconvex programming," *SIAM Journal on Numerical Analysis*, vol. 55, no. 1, pp. 168–193, 2017.
- [49] B. S. Mordukhovich and N. M. Nam, *An easy path to convex analysis and applications*. Springer, 2014.
- [50] R. T. Rockafellar and R. J.-B. Wets, *Variational analysis*. Springer Science & Business Media, 2009, vol. 317.